# *A review of the genesis, evolution, and prediction of natural fractures in deep tight sandstones of China*

**Lianbo Zeng, Lei Gong, Yunzhao Zhang, Shaoqun Dong, and Wenya Lyu**

## ABSTRACT

Natural fractures are effective reservoir spaces and the main seepage channel for tight sandstones, which control the migration, enrichment, and productivity of oil and natural gas. This paper systematically reviews the formation and distribution of natural fractures in the deep tight sandstone reservoirs of China over the past three decades. Based on geological origins, multiscale characteristics, effective evolution, and primary controllers of natural fractures, a quantitative method of natural fracture prediction was proposed. Four origins of natural fractures were identified in tight sandstone reservoirs, namely tectonic, diagenetic, tectonic-diagenetic, and overpressure origins. According to the scale and control boundary, natural fractures can be divided into four scales: large scale, mesoscale, small scale, and microscale. The multiscale natural fractures are influenced by paleotectonic stress, differences of rock mechanical property, and thickness. Controlling factors for the growth and evolution of natural fractures in tight sandstones are summarized as internal factors, dynamic factors, heterogeneity, and evolution factors, the controlling mechanisms of which on formations and distributions of natural fractures are analyzed. The effectiveness of natural fractures and the corresponding evolution are governed mainly by the formation period of natural fractures, tectonic-diagenetic coupling, abnormal high-pressure fluid, and in situ stress state. Based on the analyses on the above-mentioned fractures, a set of quantitative methods are proposed to predict the orientation and intensity of natural fractures in tight sandstones. First, the method simulates the paleotectonic stress field during the formation of natural fractures. Second, the actual rock fracture model based on the transversal anisotropy of rock mechanical properties should



Manuscript received September 12, 2022; provisional acceptance January 10, 2023; revised manuscript received January 19, 2023; final acceptance April 16, 2023.
DOI:10.1306/07052322120

## AUTHORS

LIANBO ZENG ~ *State Key Laboratory of Petroleum Resources and Prospecting, China University of Petroleum, Beijing, China; College of Geosciences, China University of Petroleum, Beijing, China; Institute of Energy, Peking University, Beijing, China; lbzeng@sina.com*

Lianbo Zeng is a professor of geology at the State Key Laboratory of Petroleum Resources and Prospecting at the China University of Petroleum, Beijing. He received his M.S. degree from the China University of Geosciences, Beijing, and his Ph.D. from the China University of Petroleum, Beijing. His interests include tectonic stress fields, natural fracture systems, and reservoir characterization. He is a corresponding author of this paper.

LEI GONG ~ *Bohai-Rim Energy Research Institute, Northeast Petroleum University, Qinhuangdao, Hebei Province, China; kcgonglei@foxmail.com*

Lei Gong is a professor of geology at the Northeast Petroleum University, Qinhuangdao, China. He received his M.S. degree and Ph.D. from the China University of Petroleum, Beijing. His current interests are the characterization, formation, and distribution of natural fractures in tight sandstone and carbonate reservoirs. He is a corresponding author of this paper.

YUNZHAO ZHANG ~ *Xi'an Petroleum University, Xi'an, Shanxi Province, China; zhangyunzhaocup@163.com*

Yunzhao Zhang received his M.S. degree and Ph.D. in geologic resources and geologic engineering from the China University of Petroleum, Beijing. He is now a postdoctoral researcher at Xi'an Petroleum University. His current interests are the characterization, formation, and distribution of natural fractures in tight sandstone reservoirs.

SHAOQUN DONG ~ *State Key Laboratory of Petroleum Resources and Prospecting, China University of Petroleum, Beijing, China; College of Sciences, China University of Petroleum, Beijing, China; dshaoqun@163.com*

Shaoqun Dong received his M.S. degree and Ph.D. in geologic resources and geologic engineering from the China University of Petroleum, Beijing. He is now an associate professor at the College of Sciences of the China University of Petroleum, Beijing. His current research interests are in the characterization and modeling of natural fractures.

WENYA LYU ~ *State Key Laboratory of Petroleum Resources and Prospecting, China University of Petroleum, Beijing, China; College of Geosciences, China University of Petroleum, Beijing, China; wylvwenwen@gmail.com*

Wenya Lyu received her B.A. degree from the China University of Geosciences, Wuhan, and a Ph.D. in geologic resources and geologic engineering from the China University of Petroleum, Beijing. She is now an associate professor at the College of Geosciences of the China University of Petroleum, Beijing. Her current research interests are in the characterization, formation, and distribution of natural fractures in tight sandstones.

## ACKNOWLEDGMENTS

The authors are particularly grateful to S. E. Laubach, P. D. Bons, A. Brogi, and the anonymous reviewers for their constructive comments and suggestions, which have improved the manuscript significantly. This study was financially supported by the National Natural Science Foundation of China (Grant Nos. U21B2062, 42072155).

be established. Third, constraint from the main controlling factors for the formation and distribution of natural fractures, the directions, and their intensities of natural fractures are predicted.

## INTRODUCTION

With increasing demands for oil and gas in the world, tight sandstones with an in situ matrix permeability of less than 0.1 md have become a primary target (Dutton and Finley, 1988; Cumella and Scheevel, 2012; Lai et al., 2018a; Gao et al., 2019; Hu et al., 2021). Tight sandstone oil and gas resources in China have great exploration potential, which has become an important area for increasing oil and gas reserves and production in recent years (Wang et al., 2018). Large-scale tight oil or gas sandstones have been found in the Jurassic and Cretaceous in the Tarim Basin, the Upper Triassic in the Sichuan Basin, the Carboniferous–Permian in the Ordos Basin, and the Paleogene in the Bohai Bay Basin (Wang et al., 2021). However, the low textural and compositional maturity of original sediments, large burial depth (most >4000 m or even >7000 m), and strong diagenesis (mechanical compaction and cementation) result in low porosity and permeability in tight sandstones (Gong et al., 2016; Lyu et al., 2017; Zucchi et al., 2017; Luo et al., 2018; Wang et al., 2018; Wu et al., 2020). Meanwhile, various types and scales of natural fractures are commonly developed in tight sandstones (Olson et al., 2009; Laubach et al., 2016; Hooker et al., 2018; Gong et al., 2019b; Liu et al., 2021a; Zeng et al., 2021; Gong et al., 2023).

The multiscale natural fracture systems play important roles in hydrocarbon accumulation and development (L. Gong, unpublished results; Lorenz et al., 1988, 2002; Dutton et al., 1993; Ozkan et al., 2011; Lyu et al., 2017; Almansour et al., 2020; Zhang et al., 2021; Zeng et al., 2022; Zucchi et al., 2022). Effective natural fractures are main seepage pathways and effective storage spaces for oil and gas (Zeng et al., 2013). However, destructive diagenesis (e.g., cementation) can degrade the effectiveness of natural fractures, which deprives the seepage and storage abilities of natural fractures (Maerten et al., 2006; Lohr et al., 2008; Rotevatn and Fossen, 2011; Liu et al., 2021b). High hydrocarbon production relies on artificial hydraulic fracturing to generate fracture networks in tight sandstones that provide essential pathways for fluid flow (Chang et al., 2020). Natural fractures influence the propagation and extent of hydraulic fracturing (Fu and Dehghanpour, 2020). Therefore, natural fractures are very important for oil and gas enrichment and development in tight sandstones (Gong et al., 2017a; Lee et al., 2018; Lyu et al., 2019; Zeng et al., 2021; Zhang et al., 2021). Meanwhile, natural fractures are also key geological factors in the evaluation of the seal integrity

of potential sites for carbon dioxide sequestration and nuclear waste disposal, where the leakage of carbon dioxide or fluid may take place along natural fractures with high permeability (Tongwa et al., 2013).

Natural fractures are typically defined as naturally occurring macroplanar discontinuities in rocks due to deformation or physical diagenesis (Aguilera, 1980; Lorenz et al., 1991; Dutton and Diggs, 1992; Peacock et al., 2016). A large number of small faults (with throw less than 5 to 10 m) cannot be directly identified by three-dimensional (3-D) seismic data, which should also be classified as natural fractures (Lohr et al., 2008; Rotevatn and Fossen, 2011; Gong et al., 2021a). Natural fractures were often classified from the aspect of failure modes (Pollard and Aydin, 1988; Fossen, 2016), mechanical properties (Kim et al., 2004; Gong et al., 2019a), and geological origins (Zeng, 2010) in tight sandstones. A series of characterization methods for natural fractures were established based on outcrops, cores, thin sections, and scanning electron microscopy (Sanderson and Nixon, 2015, 2018; Watkins et al., 2015; Cawood et al., 2017; Healy et al., 2017; Lyu et al., 2017; Miranda et al., 2018; Gong et al., 2019c; Sanderson and Peacock, 2019; Boersma et al., 2020); identifying and evaluating methods using log, drilling and production data (Narr and Lerche, 1984; Howard, 1990; Narr, 1991; Laubach, 1997; Lyu et al., 2016; Fernández-Ibáñez et al., 2018; Dong et al., 2020a–c; Liu et al., 2020); and predicting methods from curvature (Murray, 1968), geomechanical simulation (Maerten et al., 2006; Lohr et al., 2008; Camac and Hunt, 2009; Gong et al., 2021a), and seismic data (Fernández-Ibáñez et al., 2018; Boersma et al., 2020).

Many studies have proven that natural fractures are controlled by mechanical stratigraphy (Kranz, 1983; Pollard and Aydin, 1988; Underwood et al., 2003; Gross and Eyal, 2007; Laubach and Diaz-Tushman, 2011; Ferrill et al., 2014). Natural fractures are typically developed within a single lithologic layer, cutting through the same lithologic unit, and ending at the contact between this unit and its overlying or underlying lithologic units (Larsen and Gudmundsson, 2010; Smart et al., 2014; Ogata et al., 2016; Ferrill et al., 2017; McGinnis et al., 2017). A good linear relationship can be found between fracture spacing and layer thickness (Narr and Suppe, 1991; Wu and Pollard, 1995; Bai and Pollard, 2000; Chang et al., 2016; McGinnis et al., 2017). In fact, the distribution of natural fractures is much more complicated and varies greatly in size (Zeng et al., 2020; Lyu et al., 2021). Some natural fractures are not within a single lithologic layer and cut through multiple lithologic layers, the fracture height of which is much larger than a single lithologic layer thickness (Gross and Eyal, 2007; Corradetti et al., 2018). Some natural fractures only develop locally within a single lithologic layer, rather than run through the whole lithologic layer, where the natural fracture scale is smaller than the thickness of a single lithologic layer (Hooker et al., 2013; Lavenu and Lamarche, 2018). Therefore, investigating the distribution and primary controllers of multiscale fractures is crucial to understanding the development rule and their roles in tight sandstones.

Comprehensive evaluation of natural fractures is very important to the development of tight oil or gas sandstones (Zeng and Liu, 2010; Gale et al., 2014; Zanella et al., 2015; Zeng et al., 2021). Based on geological origins and main control factors, we can predict the orientation and density of natural fractures by geomechanical simulation. It provides a quantitative approach to understanding the distribution rule of natural fractures in tight sandstones.

## GENESIS AND FEATURES OF FRACTURES

According to the fractography, occurrence, and spatial distribution characteristics, four origins of natural fractures were identified in the tight sandstone reservoirs of China: tectonic, diagenetic, tectonic-diagenetic, and abnormal high-pressure origins (Figure 1) (Zeng, 2010; Zeng et al., 2022).

### Tectonic Origin

Tectonic fractures refer to fractures controlled by local tectonic events or regional tectonic stress fields (Zeng and Li, 2009; Brogi et al., 2016). They are regularly and directionally developed in tight sandstone reservoirs and can be found in various lithologies. Tectonic fractures are relatively stable in strikes at certain scales, frequently appearing as en echelon or conjugate fractures. Tectonic fractures are often semifilled or fully filled with authigenic calcite, quartz, gypsum, or other minerals. They can be subdivided into intralayer opening fractures, throughgoing shear fractures, and

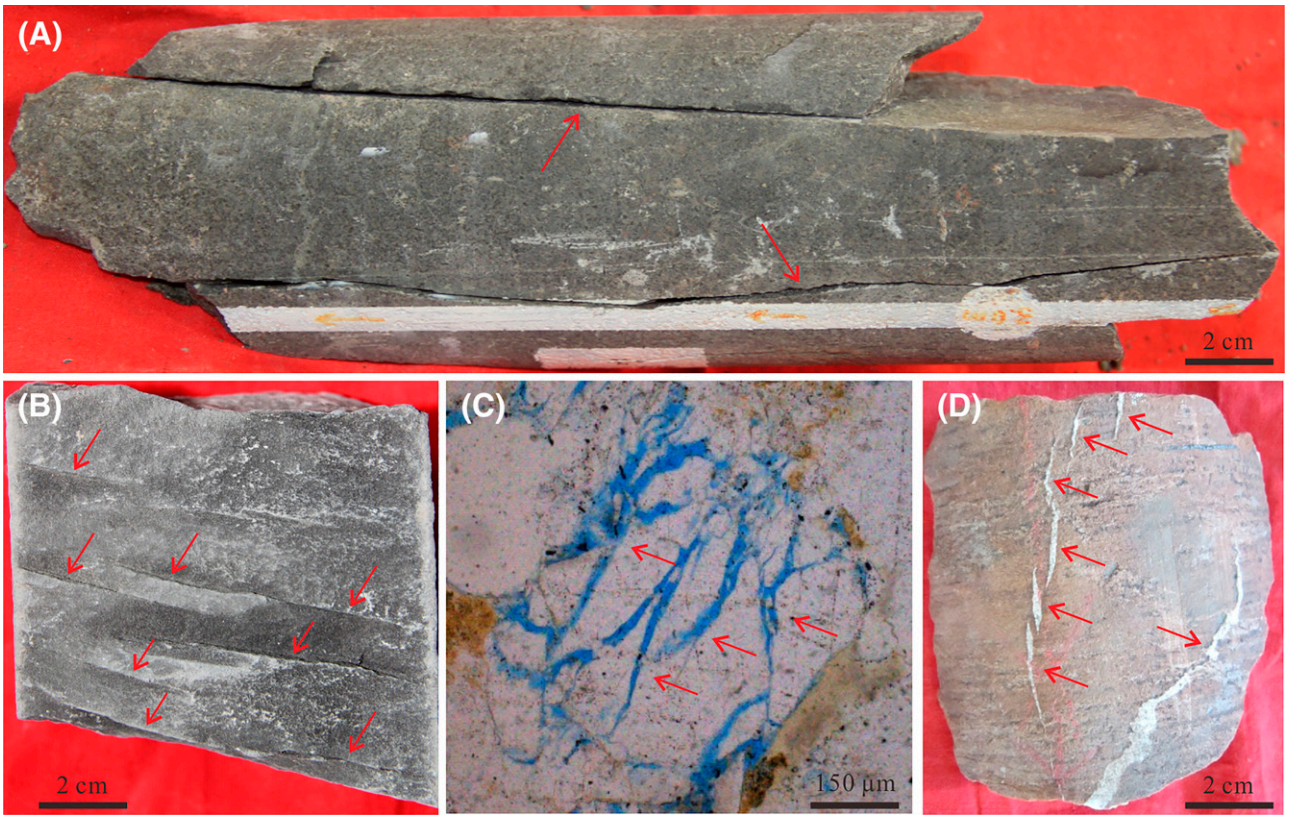


**Figure 1.** Fracture types in tight sandstone reservoirs. (A) Tectonic fractures, sandstone from the Paleogene Shahejie Formation, Bohai Bay Basin, China; (B) diagenetic fractures, sandstone from the Upper Triassic Yanchang Formation in the Ordos Basin, China; (C) tectonic-diagenetic, sandstone from the Lower Jurassic Ahe Formation in the Kuqa foreland basin, China; (D) abnormal-high pressure origins, sandstone from the Upper Cretaceous Bashijiqike Formation in the Kuqa foreland basin, China. Red arrows indicate locations of the fractures.

bedding-parallel shear fractures based on their mechanical properties and spatial coupling with bedding planes.

Intralayer opening fractures are generally controlled by mechanical stratigraphy, which are within the mechanical layer and end at its upper and lower interfaces (Gong et al., 2021b; Lyu et al., 2022). The fracture plane is typically planar and nearly vertical or intersects at a large angle with the bedding plane. These fractures are mostly filled with quartz, calcite, pyrite, or other minerals (Figure 2A). Intralayer opening fractures are widely developed in tight sandstone, and intersected fractures can be found on cores and outcrops to form fracture networks, where fractures within the same group have equal spacing.

Throughgoing shear fractures developing under shear stress have smooth surfaces with obvious scratches or steps (Figure 2B) (Gong et al., 2019a; Zeng et al., 2020). They are often arranged en echelon and penetrate mineral grains and rocks. They have a large lateral extension length and can cut through several mechanical layers in vertical, with a height of several meters to tens of meters.

Bedding-parallel shear fractures are formed due to sliding along beddings under tectonic compression, which are developed mainly in foreland thrust belts (Zeng et al., 2013; Gong et al., 2019c). Bedding-parallel shear fractures mainly develop along soft structures (e.g., sand–mudstone interfaces). These fractures are approximately parallel to or intersect with beddings at a low angle, with obvious scratches or mirror on fracture surfaces (Figure 2C, D). Weak calcite filling can be found locally, with good lateral connectivity in most positions. Fracture development is greatly affected by the dip angle of beddings (e.g., fracture size and density increase with the dip angle).

## Diagenetic Origin

Diagenetic fractures are also one of the common fracture types in tight sandstone reservoirs. The so-called

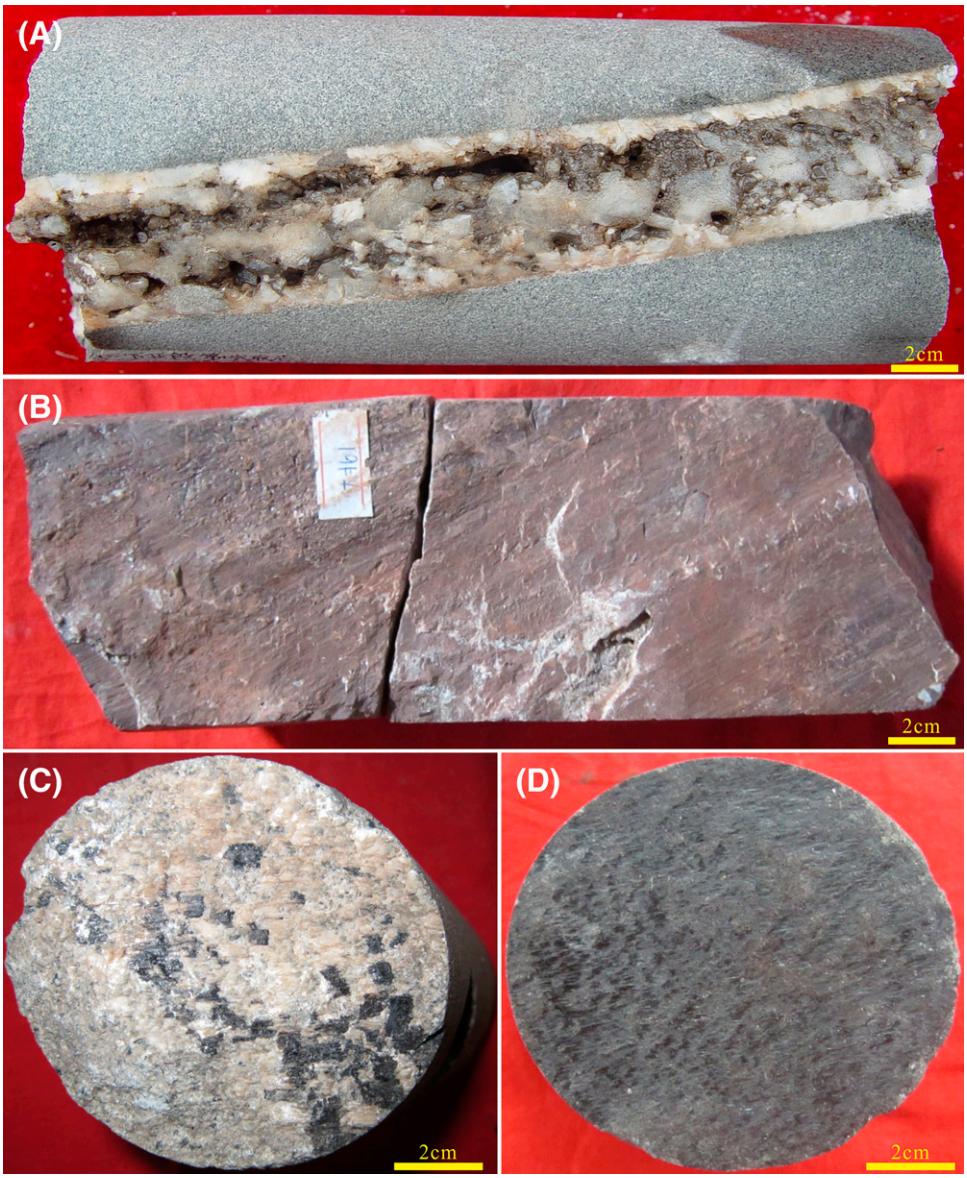


**Figure 2.** Characteristics of tectonic fractures. (A) Opening fracture filled by quartz with a width of 5 cm, sandstone from the Upper Triassic Xujiahe Formation in the Sichuan foreland basin, China; (B) throughgoing shear fracture, sandstone from the Lower Jurassic Ahe Formation in the Kuqa foreland basin, China; and (C, D) bedding-parallel shear fractures, argillaceous siltstones from the Upper Cretaceous Bashijiqike Formation in the Kuqa foreland basin, China.

diagenetic fractures refer to the nearly horizontal fractures that are derived from pressure dissolution or compaction in the diagenetic process (Zhang et al., 2020). The most common one is bedding-parallel fractures (Figure 3). Their distribution is controlled by sedimentary microfacies and diagenesis, developing mainly in fine sandstones (especially arkose sandstones) (Gong et al., 2019b). They are distributed discontinuously in horizontal or at a low angle along a microbedding plane with a small fracture aperture and coarse fracture plane. These fractures generally bypass mineral grains, presenting as tensile fractures. Most bedding-parallel fractures are not filled, with a small group being filled with mud or bitumen in local position. Bedding-parallel fractures are commonly oil bearing. For example, in the tight sandstone reservoirs of the Upper Triassic Yanchang Formation in the Ordos Basin, oil spots or oil shows can be observed on fracture surfaces, which are important controlling factors for the production of a well.

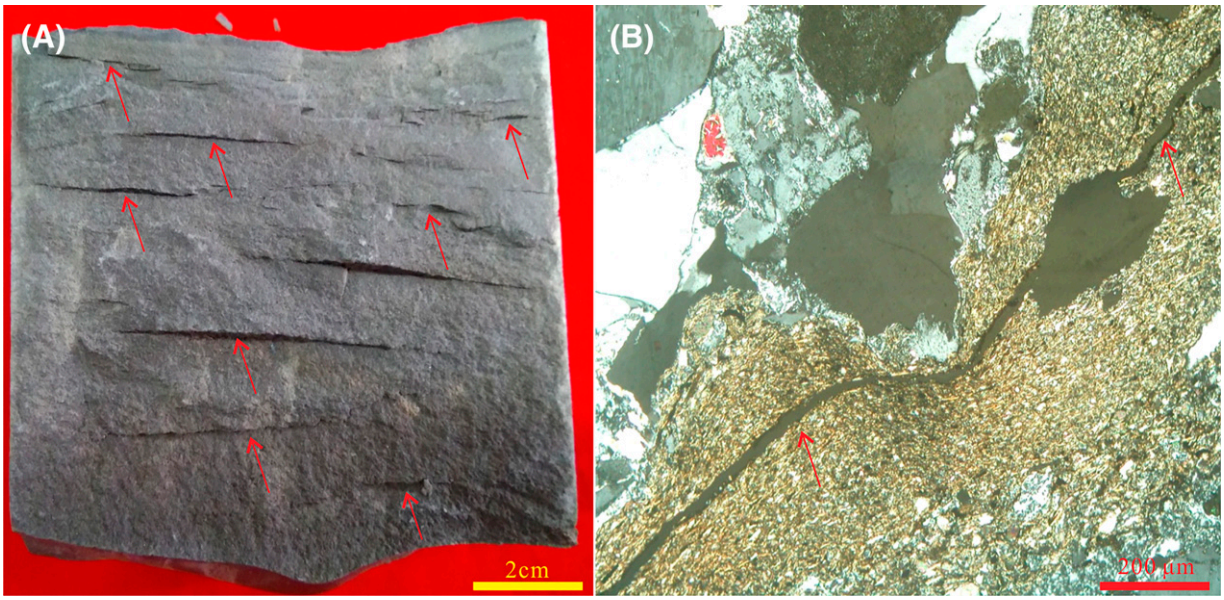


**Figure 3.** Characteristics of bedding-parallel fractures. (A) Bedding-parallel fractures on core, sandstone from the Upper Triassic Yanchang Formation in the Ordos Basin, China; (B) bedding-parallel fractures in thin sections, crossed polarized light, interface between sandstone and mudstone from the Upper Triassic Xujiahe Formation, Sichuan foreland basin, China. Red arrows indicate locations of the fractures. Modified from Zeng (2010).

### Tectonic-Diagenetic Origin

Compression among mineral grains in tight sandstone reservoirs can result in splitting within or at the edges of grains, forming intragranular fractures and grain-edge fractures (Zeng, 2010). Intragranular fractures present mainly as quartz cracks or feldspar cleavage, which develops within quartz or feldspar and other mineral grains (Figure 4A, B). These fractures are small in size and high in density, with apertures of generally less than 10 μm. Fracture density is commonly positively correlated with grain coarseness and matrix content. Grain-edge fractures are mainly distributed among mineral grains and along the edges of mineral grains (Figure 4C, D). The development of intragranular fractures and grain-edge fractures is related mainly to compaction, pressure solution, and tectonic compression during diagenesis.

### Overpressure Origin

Overpressure fractures are usually characterized by veins filled with calcite, bitumen, or other minerals and are near-horizontal (Zeng, 2010; Bons et al., 2012). Vertical or oblique veins can also be found, depending on the stress state during the fracture growth period. Most single veins are lenticular, with large width and small length (Figure 5), and some are tabular. Veins are usually several millimeters in width and several millimeters to tens of centimeters in length. The distribution of overpressure fractures is controlled by lithology and bedding, which are developed mainly in medium and coarse sandstones with relatively weak rock strength. Most overpressure fractures are nearly parallel to the bedding plane. Geometry property suggests that they are typical tensile fractures produced by tensile stress since these veins are perpendicular to the minimum principal stress. Such specific stress state is associated mainly with abnormal fluid pressure (Zeng, 2010).

## MULTISCALE CHARACTERISTICS OF NATURAL FRACTURES

### Impact of Mechanical Stratigraphy on Fracture Growth

Mechanical stratigraphy encompasses the mechanical properties, thicknesses, and interface properties of rock units (Ferrill et al., 2017; Lyu et al., 2022). Mechanical layer refers to the rock layer with similar mechanical behavior or consistent mechanical properties. It is a rock mechanical unit with the same or similar strength, brittleness, and fracture mechanical

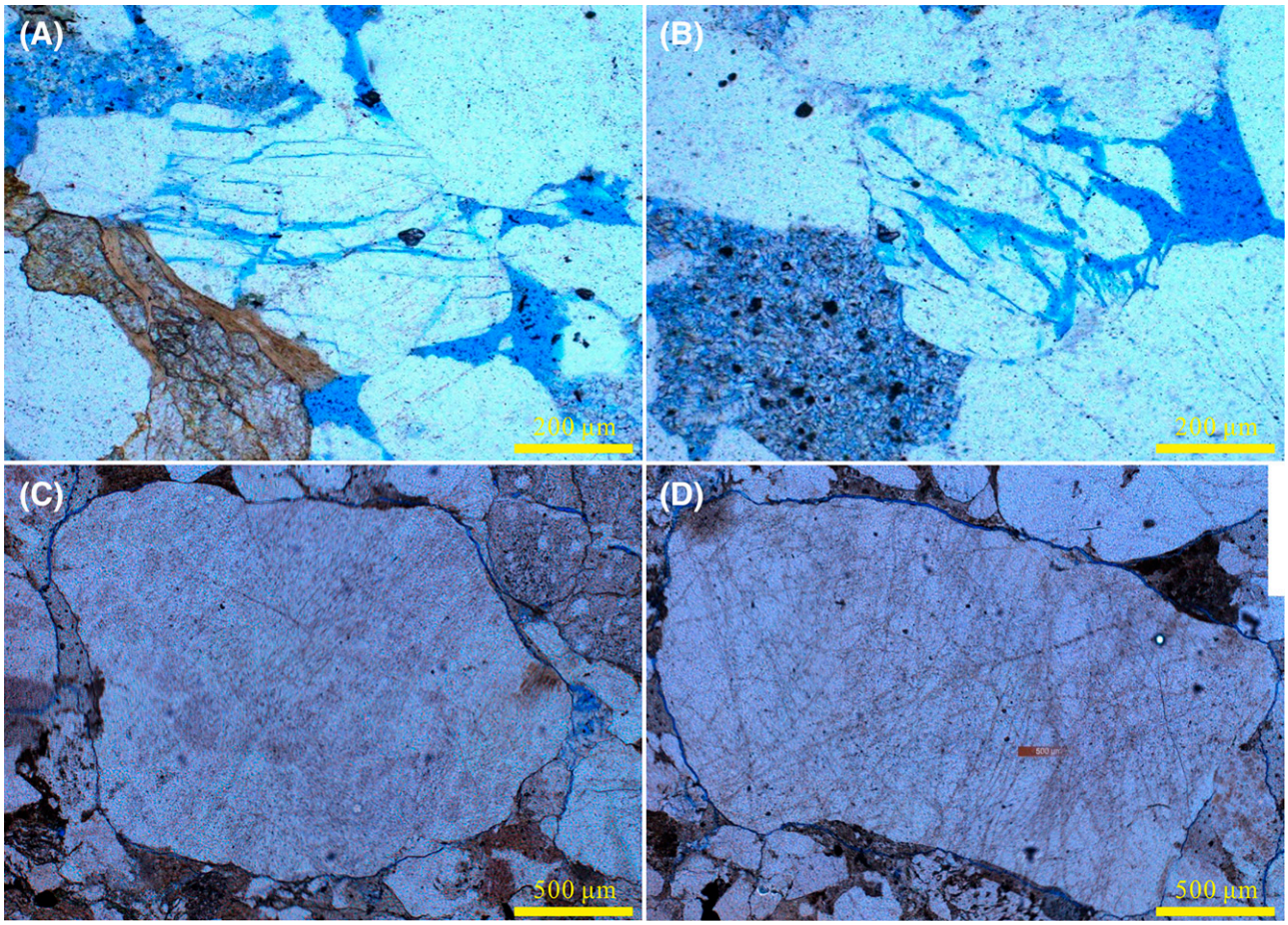


**Figure 4.** Characteristics of tectonic-diagenetic fractures. (A, B) Intergranular fractures, plane-polarized light, sandstones from the Lower Jurassic Ahe Formation in the Kuqa foreland basin, China; and (C, D) grain-edge fractures, plane-polarized light, sandstones from the Lower Jurassic Ahe Formation in the Kuqa foreland basin, China.

properties defined by the rock mechanical interface (Bertotti et al., 2007; Zeng et al., 2020).

Fracture observations from outcrops and cores confirm that mechanical stratigraphy is one of the most important factors controlling fracture types, nucleation, propagation, geometry, and spatial distribution (Narr and Suppe, 1991; Gross et al., 1995; Wu and Pollard, 1995; Underwood et al., 2003; Bertotti et al., 2007; Gross and Eyal, 2007; Laubach and Diaz-Tushman, 2011; Ferrill et al., 2017). On the one hand, mechanical stratigraphy controls fracture morphology and the development pattern. In interbedded brittle and plastic layers, fractures usually initiate (nucleate) at flaws of the mechanical interface (e.g., fossil inclusions, pyrite nodules, pores, tips, grooves, caves), then propagate in the brittle strata, and eventually terminate at the interface between brittle and plastic strata (Helgeson and Aydin, 1991; Larsen and Gudmundsson, 2010; Larsen et al., 2010; Lamarche et al., 2012; Petrie et al., 2014). These fractures controlled by mechanical stratigraphy are called bed-confined fractures (Figure 6A, B) (Gross and Eyal, 2007). In relatively homogeneous layered rocks, fractures may also end at the mechanical layer interface and deflect due to interlayer sliding and/or stripping along the interface (Larsen et al., 2010). Fractures may cut through the rock mechanical interface, where two adjacent strata have minor differences in mechanics, and form throughgoing fractures under large tectonic stress (Figure 6C, D) (Gross and Eyal, 2007; Zeng et al., 2020). On the other hand, the thickness of the mechanical layer controls fracture intensity (Narr and Suppe, 1991; Wu and Pollard, 1995; Bai and Pollard, 2000; Chang et al., 2016; McGinnis et al., 2017). The fracture spacing has a good linear relationship to the mechanical layer thickness (Narr and Suppe, 1991; Gross et al., 1995; Ferrill et al., 2017). Fracture spacing and scale increase with

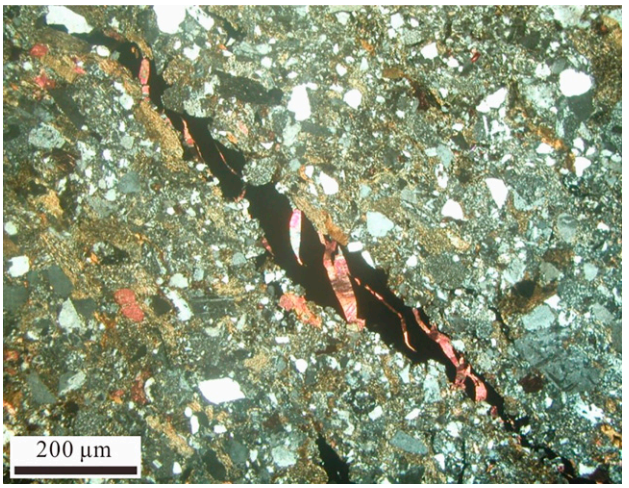


**Figure 5.** Overpressure fracture in thin section, crossed polarized light, sandstone from the Upper Triassic Xujiahe Formation, Sichuan foreland basin, China. The fracture is filled with bitumen (black) and then calcite. Calcite was filled when pore-fluid pressure dropped to 60% of static pressure in the upper strata. Modified from Zeng (2010).

the increase in mechanical layer thickness, whereas fracture density decreases with the increase in the thickness (Figure 7).

## Classification Standard of Multiscale Fractures

The mechanical stratigraphy governs the formation and distribution of natural fractures, whereas the variation in mechanical layer thickness results in multiple scales of natural fractures (Gong et al., 2018; Zeng et al., 2020). Natural fractures in oil and gas reservoirs can be divided into four levels based on their scale and related mechanical interfaces: large-scale fractures, mesoscale fractures, small-scale fractures, and microscale fractures (Figure 8; Table 1).

Large-scale fractures occur in reservoirs and generally cut both complex sand bodies and interbedded mudstone, which are commonly confined by thick mudstone interlayers. Their lengths are mainly hundreds of meters to kilometers in horizontal and tens of meters in vertical, with an aperture at the subsurface of hundreds of microns to millimeters. Such fractures usually appear as faulted fractures, which are small faults (subseismic faults) that cannot be identified from current 3-D seismic data (Zeng et al., 2021; Wang et al., 2022). The fracture number is relatively small, which works mainly as seepage channels for oil and gas rather than storage space.

Mesoscale fractures develop mainly in complex sand bodies and cut bedding planes, sedimentary discontinuities, and rhythmic lithologic interfaces, which are generally controlled by mudstone interlayers. They extend from tens of meters to hundreds of meters in horizontal and from meters to tens of meters in vertical, and have an aperture at the subsurface of hundreds of microns. They also develop in complex sand bodies and are important channels for fluid flow in tight sandstone reservoirs.

Small-scale fractures are jointed fractures that are nearly perpendicular to bedding planes. They are developed mainly in single sandstone bodies and are confined by bedding plane, sedimentary discontinuity, and rhythmic lithologic interface. The length of small-scale fractures ranges from meters to tens of meters in horizontal and decimeters to meters in vertical, whereas the underground aperture is mainly distributed between 50 and 100 μm. Small-scale fractures are developed in single sand reservoirs and are main seepage channels and effective reservoir spaces for tight sandstone reservoirs.

Microscale fractures are small in size and are commonly identified and characterized under the microscope. They are generally millimeters and centimeters in length, with underground apertures of generally less than 50 μm. Microscale fractures include bedding-parallel fractures, intragranular fractures, grain-edge fractures, and intergranular fractures. Microscale fractures are the main channels to communicate intergranular pores and intragranular pores, which can greatly improve storage space and enhance reservoir connectivity significantly. These are important for the stable production of tight reservoirs.

Studies have shown that natural fracture scale is negatively correlated with fracture number (Ortega et al., 2006; Strijker et al., 2012; Johri et al., 2014). The fracture parameters from outcrops and thin sections show that the length and aperture of fractures at different scales generally follow the power law distribution (Figure 9), whereas specific parameters of the distribution model vary with regions and tectonic backgrounds (Odling, 1997; Mi et al., 2023). The 3-D geological modeling of multiscale fractures can be realized based on the power law distribution of fractures at different scales (Maerten et al., 2006; Gong et al., 2019c).

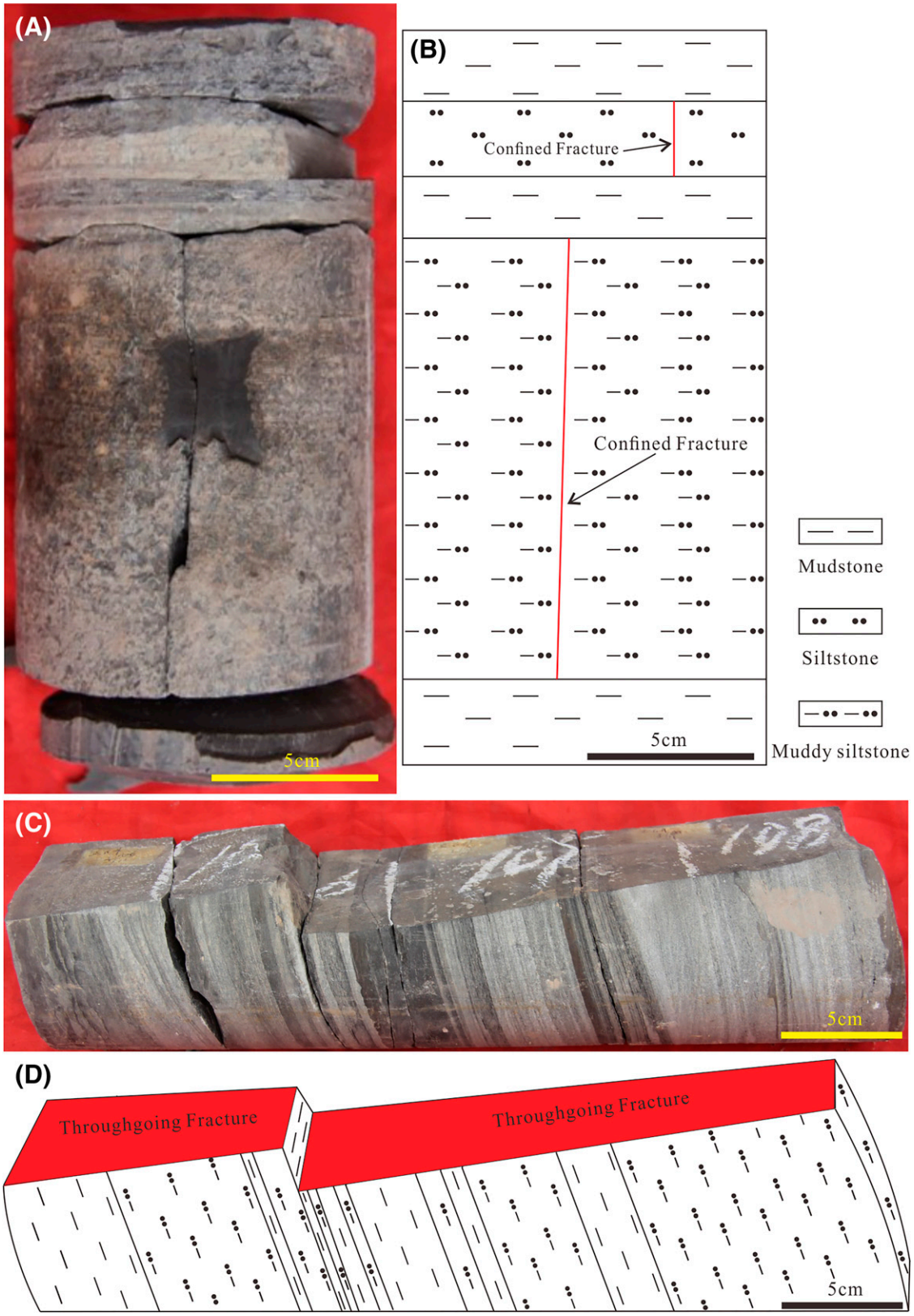


**Figure 6.** (A, B) Bed-confined fractures; and (C, D) throughgoing fractures on cores. (A, C) Cores from the Upper Triassic Yanchang Formation in the Ordos Basin, China. (B, D) Sketches of (A) and (B), respectively.

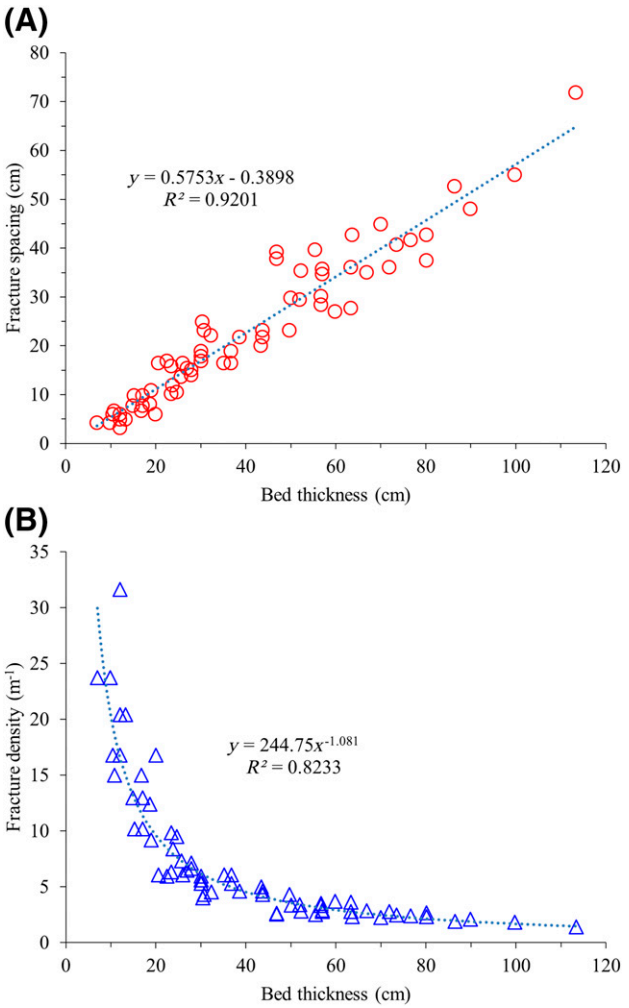


**Figure 7.** Relationship between mechanical layer thickness and fracture intensity. Data are obtained from Jurassic outcrops in the Kuqa foreland basin. (A) Relationship between mechanical layer thickness and fracture spacing; and (B) relationship between mechanical layer thickness and fracture density. $R^2$ = coefficient of determination.

## Geological Conditions of Multiscale Fracture Development

Different levels of the mechanical layer interface result in multiscale fractures (Gross and Eyal, 2007; Larsen et al., 2010; Lamarche et al., 2012; Forbes Inskip et al., 2020; Zeng et al., 2020). The occurrence of multiscale mechanical layer interfaces in the same area can be explained by geological conditions (e.g., the thickness and strength of rock mechanical interfaces and paleotectonic stresses) during the formation of natural fractures. To reflect the controlling effect of rock mechanical interface properties on fracture formation under different geological conditions, on the basis of the mechanical layer conceptual model and boundary stress established with the Yanchang Formation in Ordos Basin, China, Zeng et al. (2020) simulated the fracture development and evolution through combining finite element numerical simulation and fracture mechanics models and, consequently, established relationships between fracture development and rock mechanical properties, interlayer thickness, and tectonic stress (Figure 10). The mechanical layer model is composed of a sandstone layer and a mudstone interlayer. By changing the elastic modulus ratio (0.2, 0.4, 0.5, 0.6, 0.75, and 0.9), the thickness ratio (0.02, 0.2, and 1.0) between the sandstone layer and the mudstone layer, and boundary stress (80, 85, 90, and 95 MPa), the control effect of the mechanical property and the thickness of the interlayer and tectonic stress on fracture development can be reflected.

As Figure 10 shows, under certain tectonic stresses, the required interlayer thickness limiting fracture propagation decreases with the increasing difference in mechanical properties between sandstones and interbedded mudstones. The required difference in mechanical properties between sandstones and mudstones or required mudstone thickness is positively correlated with tectonic stress.

## CONTROLLING FACTORS OF NATURAL FRACTURE EVOLUTION

Fracture intensity statistics (e.g., fracture frequency, linear density, areal density) from outcrops, cores, thin sections, and log data suggests that natural fracture development in tight sandstone reservoir varies greatly among different regions or different horizons in the same region (Zeng and Li, 2009; Gong et al., 2019a; Lyu et al., 2019; Gao et al., 2020; Liu et al., 2020; Zeng et al., 2022). Elements affecting fracture development and evolution in tight sandstone reservoirs can be summarized as follows: internal (i.e., structure of rocks or strata) (Fossen, 2010; Ameen et al., 2012; Zeng et al., 2013, 2022; Philit et al., 2018; Gong et al., 2019b; Awdal et al., 2020; Braathen et al., 2020; Rodrigues et al., 2021); dynamic (e.g., tectonic movements, fluid) (Kim and Sanderson, 2005; Faulkner et al., 2010; Zeng and Liu, 2010; Bons et al., 2012; Johri et al., 2014; Choi et al., 2016; Peacock et al., 2016; Gao et al., 2020; Liu et al., 2020;

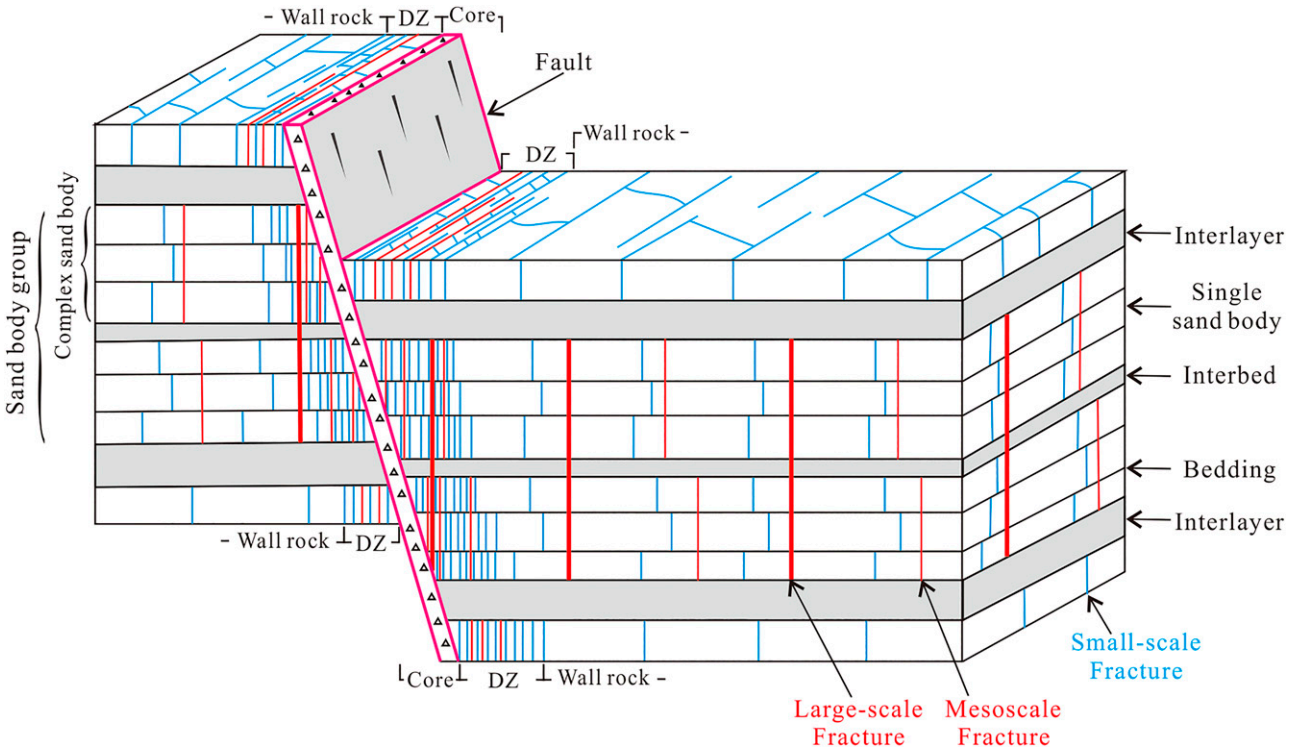


**Figure 8.** Distribution model of multiscale fractures. DZ = damage zone.

**Table 1.** Characteristics of Fractures at Different Scales

| Fracture Scales | Distribution Characteristics | Fracture Types | Length | Aperture | Role |
|---|---|---|---|---|---|
| Large scale | Cut complex sand body and interbedded mudstone, being confined by thick mudstone interlayer | Small fault, throughgoing shear fracture | Hundreds of meters to kilometers in horizontal, tens of meters in vertical | Hundreds of microns to millimeters | Seepage channel |
| Mesoscale | Cut sand body and bedding plane, but develop within complex sand body, being confined by interbedded mudstone | Throughgoing shear fracture | Tens to hundreds of meters in horizontal, meters to 10 m in vertical | Hundred-microns scale | Seepage channel |
| Small scale | Develop within single sand body, being confined by bedding plane | Intralayer opening-mode fracture | Meters to tens of meters in horizontal and decimeters to meters in vertical | 50–100 μm | Seepage channel and storage space |
| Microscale | Develop within single sand body with small scale | Bedding-parallel fracture, intergranular fracture, intragranular fractures, and grain-edge fracture | Millimeters to centimeters | <50 μm | Storage space and connect intergranular pores |

Modified from Zeng et al. (2020).

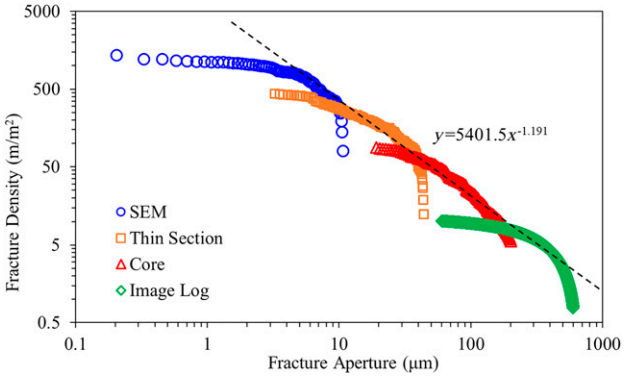


**Figure 9.** Power law distribution of multiscale fracture density; data from the Paleogene of the Bohai Bay Basin, China. All of the curves of each scale shows a lognormal distribution. When all of the data are combined, they obey a power-law distribution with an exponent of 1.191. SEM = scanning electron microscopy.

Hansberry et al., 2021; Lao et al., 2021; Mao et al., 2022); heterogeneity (rock mechanical properties and existing fractures) (Zeng et al., 2008; Gao et al., 2015; Fossen, 2016; Gong et al., 2019b); and evolution (stress state) (Ferrill et al., 2021).

## Internal Factors

### Lithology

Lithology is the basic factor of fracture development in tight sandstone reservoirs (Ameen et al., 2012; Zeng et al., 2013; Gong et al., 2019a). First, rock porosity determines its deformation mode. Specifically, particle rearrangement, breakage, and pore collapse are common in highly porous sandstone, forming deformation bands and decreasing porosity and permeability (Figure 11A, B) (Fossen and Bale, 2007; Fossen, 2010; Fossen et al., 2011; Lai et al., 2018b; Philit et al., 2018; Awdal et al., 2020; Braathen et al., 2020; Rodrigues et al., 2021). Fracture growth occurs mainly in low-porous sandstone, improving the reservoir quality greatly (Figure 11A, B). An obvious negative correlation can be found between fracture density and matrix porosity (i.e., the smaller the porosity, the higher the fracture density) (Figure 12A) (Gong et al., 2017b).

Rock mechanical property varies greatly with mineral composition and rock structure, resulting in different fracture behaviors under the same tectonic stress. Strong rock with a high elastic modulus is generally brittle, which is easily broken compared with soft rock. Mineral composition in sandstone not only controls fracture abundance but also influences filling behavior in fractures. Under the same tectonic stress, fracture density in rocks with high brittle components (e.g., quartz, calcite, dolomite) is relatively high (Figure 12B, C), whereas it is relatively low in rocks with a high plastic mineral content (e.g., clay minerals) (Figure 12B, D). Statistical data also show that fractures in sandstone with high carbonate mineral content are commonly fully filled with calcite (Gale et al., 2014; Gong et al., 2021b). Fractures in sandstone dominated by quartz, feldspar, and other minerals are partially filled, mainly unfilled, or semi-filled with authigenic quartz (Figure 12B) (Gale et al., 2014; Gong et al., 2021b).

In terms of rocks with the same composition, fractures are commonly well developed in fine-grained rocks, whereas they are poorly developed in coarse-grained rocks (Figure 12E) . This is because small pore volume and grain size can compress the rock body and decrease rock volume, increasing its rock strength greatly. Consequently, rock with low porosity and fine grains can be easily fractured under a small strain. Furthermore, sorting behavior can also control fracture density. In general, fractures are well developed in well-sorted sandstone compared with poorly sorted argillaceous sandstone (Ameen et al., 2012).

### Sedimentary Microfacies

Sedimentary microfacies has significant influence on fracture density because it controls reservoir distribution (e.g., rock composition, grain size, bed thickness)

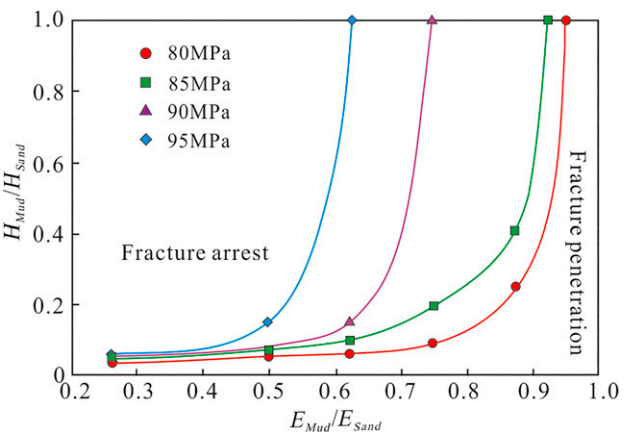


**Figure 10.** Relationship between fracture propagation and tectonic stress, difference in mechanical properties, and interlayer thickness. Modified from Zeng et al. (2020). $E_{mud}/E_{sand}$ = elastic modulus ratio between the mudstone layer and the sandstone layer; $H_{mud}/H_{sand}$ = thickness ratio between the mudstone layer and the sandstone layer.

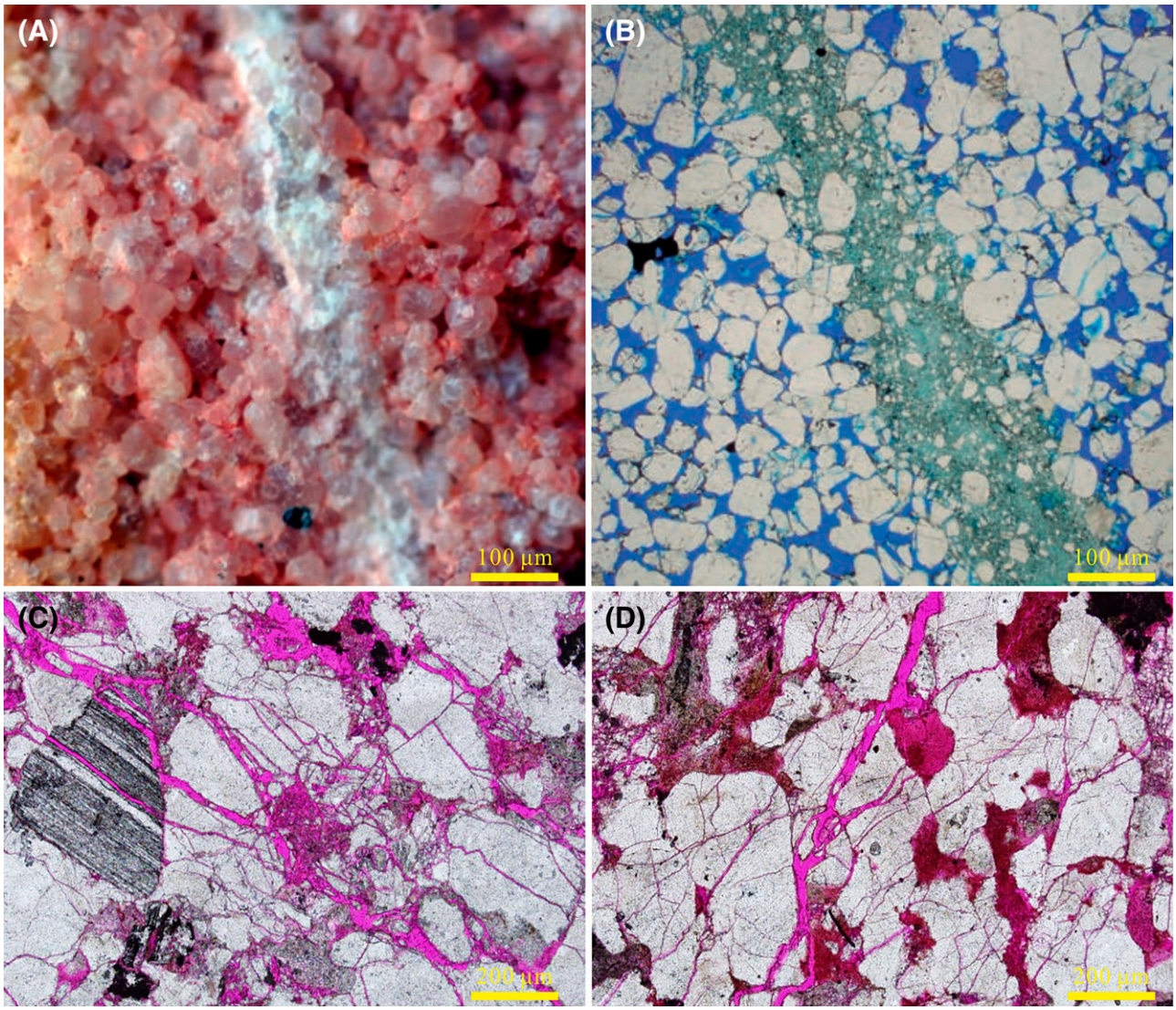


**Figure 11.** Deformation of rocks with different porosity. (A, B) Highly porous sandstone, deformation bands, decreasing rock porosity, and developing seepage barrier (modified from Fossen, 2016); and (C, D) tight sandstones and fractures can improve reservoir quality; sandstones from the Upper Cretaceous Bashijiqike Formation in the Kuqa foreland basin, China.

(Gong et al., 2017a). Here, a case from the Kuqa foreland basin (Table 2) is an example.

Fracture density data from Cretaceous cores of different sedimentary microfacies at 41 wells in the Kuqa foreland basin (Table 2) show that it is the highest at delta-front underwater interdistributary bay and front sheet, followed by delta-front underwater distributary channel, mouth bar and distributary channel, and then braided distributary channel, and it is the lowest at prodelta and floodplain swamp. This is because sandstone from delta-front underwater interdistributary bay and front sheet has fine grains, small single-layer thickness, but large cumulative thickness, which is beneficial for fracture development under the same stress conditions. However, sandstone from the delta-front underwater distributary channel, mouth bar, and distributary channel have coarse grains, mainly pebbly sandstone and sandstone, and has a large single-layer thickness, which is negative for fracture development. In braided distributary channel deposits, grains become coarser with larger thickness, mainly thick conglomerate and grainy sandstones. Prodelta and floodplain swamp have the worst fracture development because of argillaceous deposits.

## Diagenetic Facies

Diagenetic facies refer to deposits experiencing diagenetic evolution under certain diagenesis and tectonic

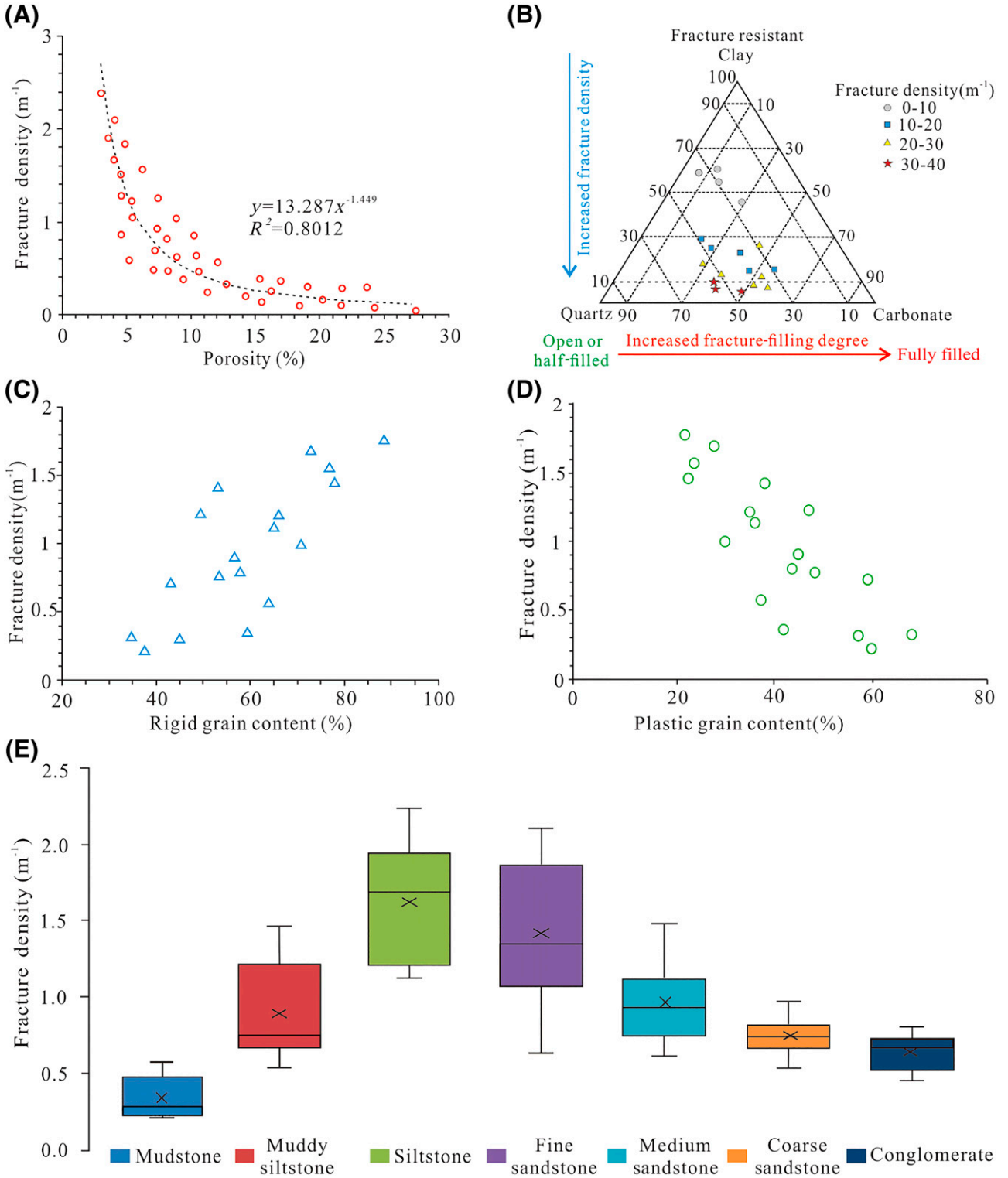


**Figure 12.** Impact of lithology on fracture growth; the data are from the Yanchang Formation of the Upper Triassic in Ordos Basin, China. (A) Relationship between porosity and fracture density; (B) relationship between mineral components and fracture abundance or filling behaviors; (C) relationship between rigid grain content and fracture density; (D) relationship between plastic grain content and fracture density; and (E) impact of grain size and mineral composition on fracture growth. $R^2$ = coefficient of determination.

**Table 2.** Fracture Density of Various Cretaceous Sedimentary Microfacies

| Sedimentary Facies | Sedimentary Subfacies | Sedimentary Microfacies | Lithology | Macrofracture Density | Microfracture Density |
|---|---|---|---|---|---|
| Fan delta | Fan delta plain | Braided distributary channel | Dominated by thick conglomerate and grainy sandstone | 0.96 $m^{-1}$ (0.29 $ft^{-1}$) | 0.20 $cm/cm^2$ (1.29 $in./in.^2$) |
| | | Floodplain swamp | Thin interbedded silt sandstone, clay, and fine sandstone | 0.51 $m^{-1}$ (0.16 $ft^{-1}$) | 0.11 $cm/cm^2$ (0.71 $in./in.^2$) |
| | Fan delta front | Underwater distributary channel | Dominated by pebbly sandstone and sandstone | 1.58 $m^{-1}$ (0.48 $ft^{-1}$) | 0.33 $cm/cm^2$ (2.13 $in./in.^2$) |
| | | Underwater interdistributary bay | Interbedded light-gray fine sandstone, silt sandstone and grayish-green mudstone | 2.49 $m^{-1}$ (0.76 $ft^{-1}$) | 0.51 $cm/cm^2$ (3.29 $in./in.^2$) |
| | | Mouth bar | High sand content, well-sorted fine to medium sandstone | 1.66 $m^{-1}$ (0.51 $ft^{-1}$) | 0.35 $cm/cm^2$ (2.26 $in./in.^2$) |
| | | Front sheet sand | Thin sheet sand body, fine sandstone, interbedded sandstone, and mudstone | 2.65 $m^{-1}$ (0.81 $ft^{-1}$) | 0.53 $cm/cm^2$ (3.42 $in./in.^2$) |
| | Profan delta | Prodelta | Interbedded mudstone, argillaceous siltstone, calcareous shale, and oil shale | 0.49 $m^{-1}$ (0.15 $ft^{-1}$) | 0.12 $cm/cm^2$ (0.77 $in./in.^2$) |

movements, including comprehensive elements (e.g., rock grains and structure, cements, pores, fractures) (Zou et al., 2008; Lai et al., 2018a). Fracture growth varies as a function of diagenetic phases, cement types, dissolution intensity and physical properties (Laubach and Diaz-Tushman, 2011; Gong et al., 2015) confirmed that mechanical stratigraphy was not exactly the same with fracture stratigraphy. Fracture stratigraphy can express mechanical stratigraphy of the rock during fracture development, whereas mechanical stratigraphy varies with diagenetic evolution. Therefore, the influence of diagenesis on mechanical stratigraphy should be considered, and mechanical stratigraphy and fracture stratigraphy should be distinguished when predicting fractures. The influence of diagenesis on fracture growth in sandstones can be summarized in the following paragraphs.

First, continuous diagenesis changes pore structure, porosity, and mechanical properties, resulting in the rock deformation mode changing from plastic deformation, deformation band to fracture deformation (Laubach et al., 2010, 2019; Gong et al., 2015).

Second, intensive mechanical compaction can break rock, forming diagenetic fractures (e.g., bedding fractures, intragranular fractures, grain-edge fractures) and so on. Strong mechanical compaction compresses quartz and feldspar grains, making fractures along feldspar cleavage, whereas quartz cracks to form intragranular fractures and grain-edge fractures (Gong et al., 2015; Zeng et al., 2022). The differences between intragranular fractures derived from diagenetic compaction and structural compression are as follows: (1) the diagenetic compaction fractures can only develop in contacted grains, perpendicular to the contact surface, whereas the latter does not have this obvious feature; (2) the structural compression fractures are generally oriented, which are usually parallel to the intergrain fractures formed by tectonic movement; (3) the diagenetic compaction fractures generally are of small size, have a short extension, and often do not cross the whole grains, whereas the latter generally cross the whole grains; and (4) the former is generally developed early, whereas the latter is typically developed in later stages and cut the former.

**Table 3.** Fracture Density of Different Diagenetic Facies at Cretaceous Rocks in Kuqa Foreland Basin

| Diagenetic Facies | Diagenetic Phase | Reservoir Property | | Fracture Density | |
|---|---|---|---|---|---|
| | | Porosity, % | Permeability, md | Macrofractures | Microfractures |
| Strongly cemented and compacted unit | | | | | |
| Calcite-cemented zone in the west | Middle diagenesis-$A_2$ | 5.17 | 1.45 | 1.14 $m^{-1}$ (0.35 $ft^{-1}$) | 0.35 $cm/cm^2$ (2.26 $in./in.^2$) |
| Calcite-dolomite cemented zone in the middle | Middle diagenesis-B | 2.65 | 0.08 | 1.97 $m^{-1}$ (0.60 $ft^{-1}$) | 0.52 $cm/cm^2$ (3.35 $in./in.^2$) |
| Calcite-cemented zone in the east | Middle diagenesis-$A_2$ | 4.20 | 0.33 | 1.43 $m^{-1}$ (0.44 $ft^{-1}$) | 0.44 $cm/cm^2$ (2.84 $in./in.^2$) |
| General cemented and compacted unit | | | | | |
| General calcite- gypsum cemented zone | Middle diagenesis-$A_2$ | 13.21 | 47.12 | 0.93 $m^{-1}$ (0.28 $ft^{-1}$) | 0.32 $cm/cm^2$ (2.06 $in./in.^2$) |
| General calcite- cemented zone | Middle diagenesis-$A_2$ | 11.14 | 47.64 | 0.87 $m^{-1}$ (0.27 $ft^{-1}$) | 0.31 $cm/cm^2$ (2.00 $in./in.^2$) |
| Weakly cemented and strongly dissolved unit | Middle diagenesis-$A_1$ | 18.69 | 428.10 | 0.59 $m^{-1}$ (0.18 $ft^{-1}$) | 0.18 $cm/cm^2$ (1.16 $in./in.^2$) |

Third, diagenetic facies control structural fracture development (Gong et al., 2015; Lyu et al., 2017). Compaction and cementation can give rise to tight rock and increase rock strength, which contribute fracture deformation under small strain. However, dissolution can increase porosity in rocks, which is unfavorable to fracture development. For example, fracture density determined from 1399.52-m (4590.43-ft) cores and 188 thin sections of different diagenetic facies at the Cretaceous from 28 wells in the Kuqa foreland basin (Table 3) shows that the strongly cemented and compacted diagenetic facies have the highest fracture density. The average linear density of the macrofractures is 1.51 $m^{-1}$ ([0.46 $ft^{-1}$] with the maximum value up to 5.57 $m^{-1}$ [1.70 $ft^{-1}$]), and the average area density of the microfractures is 0.44 $cm/cm^2$ (2.84 $in./in.^2$). The second is the general cemented and compacted diagenetic facies, with an average linear density and an average area density of macrofractures of 0.93 $m^{-1}$ (0.28 $ft^{-1}$) and 0.32 $cm/cm^2$ (2.06 $in./in.^2$), respectively. Poorly cemented and strongly dissolved diagenetic facies have high-quality reservoir and poorly developed fractures, where the average linear density of the macrofractures is only 0.59 $m^{-1}$ (0.18 $ft^{-1}$) and the average area density of the microfractures is 0.18 $cm/cm^2$ (1.16 $in./in.^2$).

## Dynamic Factors

### Structure

Structure can affect fracture development in tight sandstone reservoirs by controlling local stress distribution in different structural units (Brogi, 2011; Gao et al., 2020; Liu et al., 2020; Brogi et al., 2021). Fault is an important external factor controlling fracture development in tight reservoirs via stress perturbation during fault activity. Obvious stress concentration always occurs along fault zones, and fractures develop. Faults can generally be divided into two units: fault core and damage zones (Figure 13A) (Kim and Sanderson, 2005; Faulkner et al., 2010; Torabi and Berg, 2011; Johri et al., 2014; Choi et al., 2016; Peacock et al., 2016; Hansberry et al., 2021; Lao et al., 2021). The fault core is generally composed of sliding surface, fault gouge, breccia, structural lens, cataclasite, or ultracataclasite. The damage zone is generally composed of multiscale fractures and secondary faults.

Observed fracture development around faults on outcrops shows that fractures are well developed, with small spacing at the fault core, especially at the ends, intersections, and overlapping sections. Fracture density decreases in a negative exponential trend with its distance from the fault core, which tends to be stable at certain distances. The damage zone can

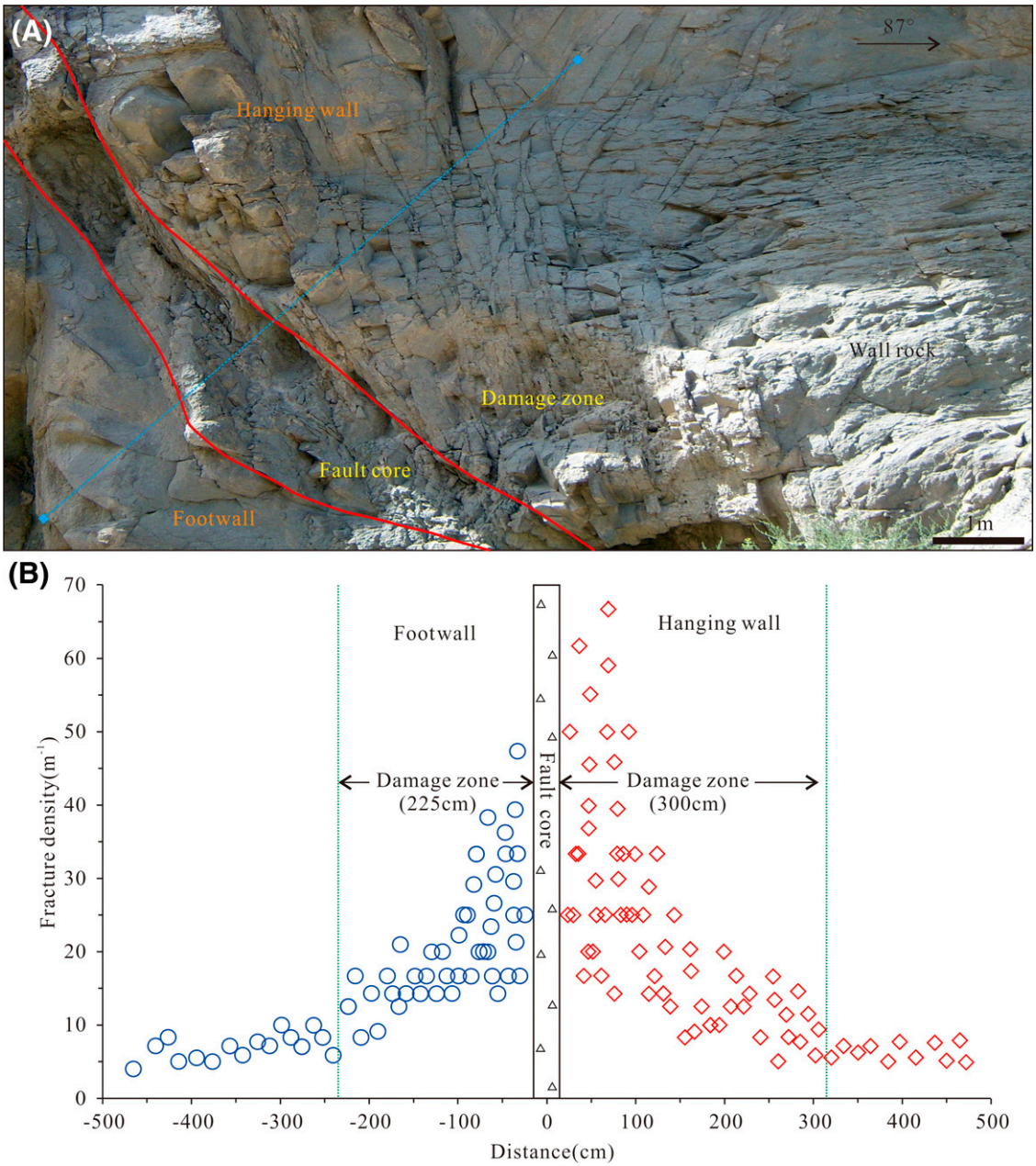


**Figure 13.** (A) Distribution of the fracture system within a fault zone from the Lower Jurassic tight sandstones in the Kuqa foreland basin, western China. (B) Fracture density distribution along the blue dotted line in (A).

be identified when the fracture density is consistent with the regional fracture density (Figure 13B). The width of the damage zone is proportional to the fault displacement—that is, the greater the fault displacement, the larger the width of the damage zone. However, the growth rate of the width decreases when the displacement is too large (after hundreds of meters of displacement) (Faulkner et al., 2010; Choi et al., 2016). Furthermore, although the linear density of fractures in both hanging wall and footwall decreases significantly with increasing distance from the fault, fracture density in the hanging wall is significantly higher than that in the footwall because the hanging wall is commonly an active one with intensive stress disturbance.

The distribution of fractures in fault-bend fold is more complex in foreland basin. Layer-parallel shortening–related fractures, interlayer slipping–related fractures, active hinge parallel shearing–related fractures, and curvature-related fractures are

found in fault-bend fold (Mao et al., 2022). The layer-parallel shortening–related fractures and interlayer slipping–related fractures are well developed in mechanical stratigraphy, whereas the active hinge parallel shearing–related fractures and curvature-related fractures are not strictly confined by mechanical stratigraphy. Based on the data of discrete element simulation and outcrops, fractures in fault-bend fold can be divided into six domains (A–F). The layer-parallel shortening–related fractures and interlayer slipping–related fractures are most developed in domain B, followed by domains E, C, and D. The active hinge parallel shearing–related fractures and curvature-related fractures are mainly developed in domains C and E, respectively (Figure 14).

## Pore Pressure

Abnormal high pressure is an important driving force for fracture development in tight reservoirs (Gudmundsson, 1999; Cox, 2010; Zeng and Liu, 2010; Bons et al., 2012; Zanella et al., 2015; Lyu et al., 2019; Gong et al., 2021b). The occurrence of abnormal fluid pressure in rock can decrease effective stress under large differential stress, and move the Mohr circle to intersect with the fracture envelope, which is conducive to the shear fracture growth (Figure 15A). A good positive correlation can be observed between fracture linear density and the formation pressure coefficient (Figure 15B), indicating the contribution of abnormal high pressure to fracture development. Continuous increasing pore fluid pressure

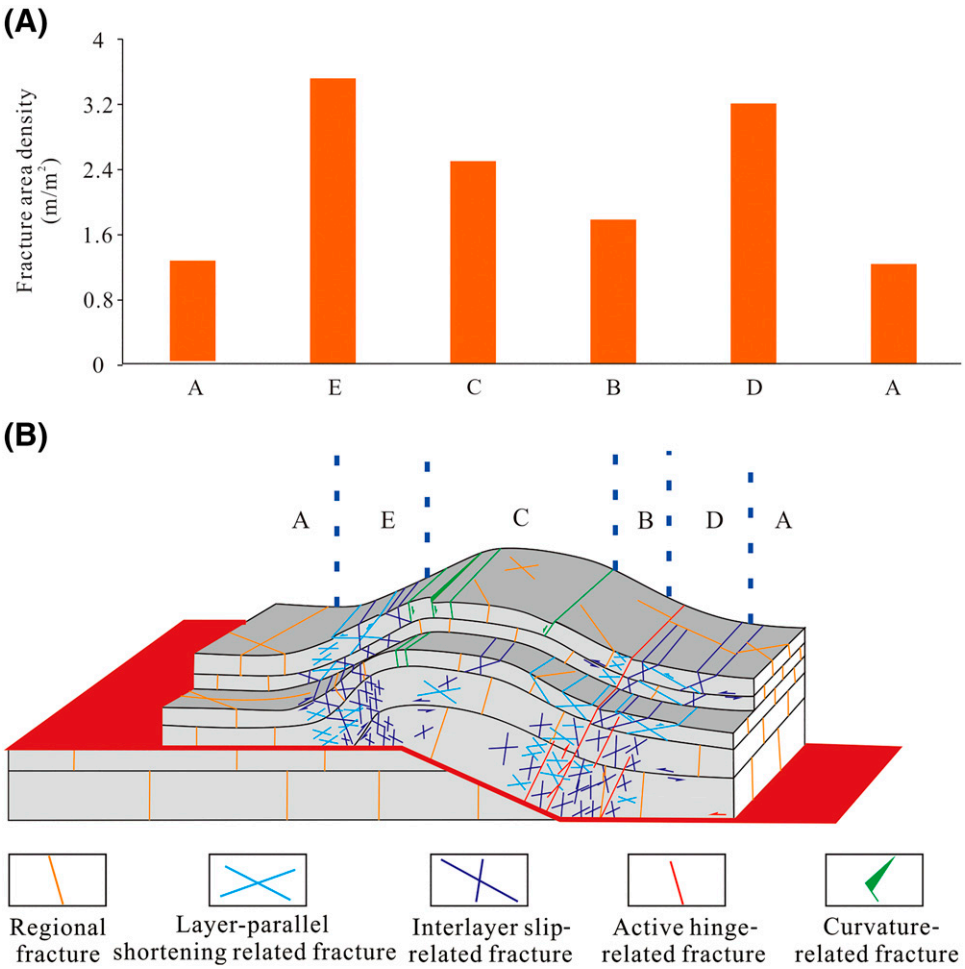


**Figure 14.** Fracture domain in the fault-bend fold (modified from Mao et al., 2022). (A) Fracture area densities in domains A–E of the fault-bend fold measured from outcrops in the southern margin of the Junggar Basin, western China. (B) Fracture development pattern of the fault-bend fold integrated with discrete element simulation and outcrops. Five deformation panels are developed in this pattern: unfolded layer (panel A), weakly folded layer in backlimb (panel B), fold core (panel C), strongly folded layer in backlimb (panel D), and forelimb (panel E). The fracture intensity increased sequentially in the panels. For the specific fracture characteristics of different panels, see Mao et al. (2022).

can alter the minimum effective principal stress from extrusion state to extension state when the differential stress is small, forming overpressure fracturing that is often filled with calcite and bitumen to form tensile fracture veins. Therefore, fluid in pores can transform compressive stress in the thrust zones into tensile stress, developing tension fractures related to abnormal high pressure under compressional stress environments. This is the main reason why not only shear fractures but also tension fractures are widely developed in the thrust zone and deep-buried reservoirs.

The poroelastic effect also contributes to the formation and propagation of fractures in porous rocks (Fossen, 2016). Because the cemented grain contacts are elastic, some of the pore fluid pressure ($P_f$) is taken up by elastic deformation. Thus, the increase in stress ($\Delta\sigma_n$) against the fracture wall will not be equal to $P_f$, but will be less by an amount that depends on the porosity of the porous rocks (Fossen, 2016):

$$\Delta\sigma_n = \varphi p_f + (1-\varphi)\alpha P_f \quad (1)$$

The factor $\alpha$ (<1) is known as the Biot poroelastic parameter and characterizes the poroelastic effect. Since $\alpha$ is less than 1, the normal stress acting on the fracture wall is less than the pore fluid pressure within the fracture, so the fracture wall is under tension. As the pore pressure increases, the tensile stress is concentrated at the fracture tips, and the fracture will grow until the pore fluid pressure within the fracture drops (as the fracture volume increases) to equal the normal stress on the fracture wall.

## Heterogeneity

### Heterogeneity of Rock Mechanical Properties

The heterogeneity of rock mechanical properties is an important factor influencing fracture development in different directions, especially under homogenous tectonic stress (Zeng et al., 2008; Gao et al., 2015). Traditional rock mechanics analysis mostly simplified rocks as anisotropic in vertical and as isotropic in lateral. Zeng et al. (2008) confirmed rock mechanical property anisotropy in lateral through performing rock mechanics experiments on elastic modulus, Poisson's ratio, and uniaxial compressive strength in different directions, and held that anisotropy under some geological conditions is too strong to be simplified as lateral isotropy. Gao et al. (2015) and Gong

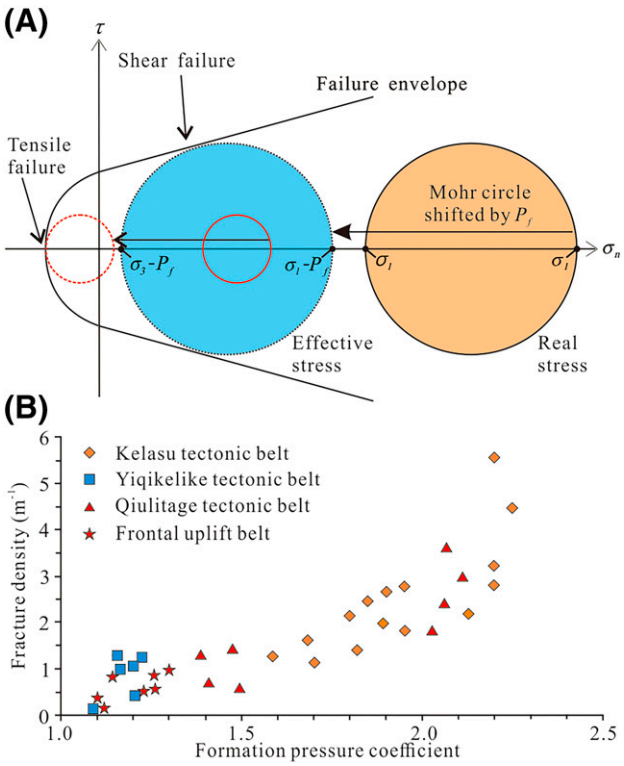


**Figure 15.** (A) Schematic diagram of formation mechanism of overpressure fracture; and (B) relationship between fracture linear density and formation pressure coefficient.

et al. (2019b) used the Upper Triassic Yanchang tight sandstone reservoir at Ordos Basin as an example, carried out uniaxial and triaxial rock mechanical tests and acoustic emission tests to confirm the existence of rock mechanical property (tensile strength, compressive strength, elastic modulus, and Poisson's ratio) anisotropy in different directions (Figure 16), and analyzed its influence on fracture development. The anisotropy of rock mechanical properties plays a significant role in the fracture development degree in different directions. It usually inhibits one group of conjugate shear fracture and leaves another group, resulting in the inconsistent development of conjugate shear fractures (Figure 17). Different rock microstructures in different directions bring uneven internal stress states, fracturing rock along the lowest strength under the same tectonic stress.

### Preexisting Fractures

Tight sandstone reservoirs commonly experience multiple tectonic movements. Existing fractures derived from variation and superposition of the stress field in different periods can influence fracture

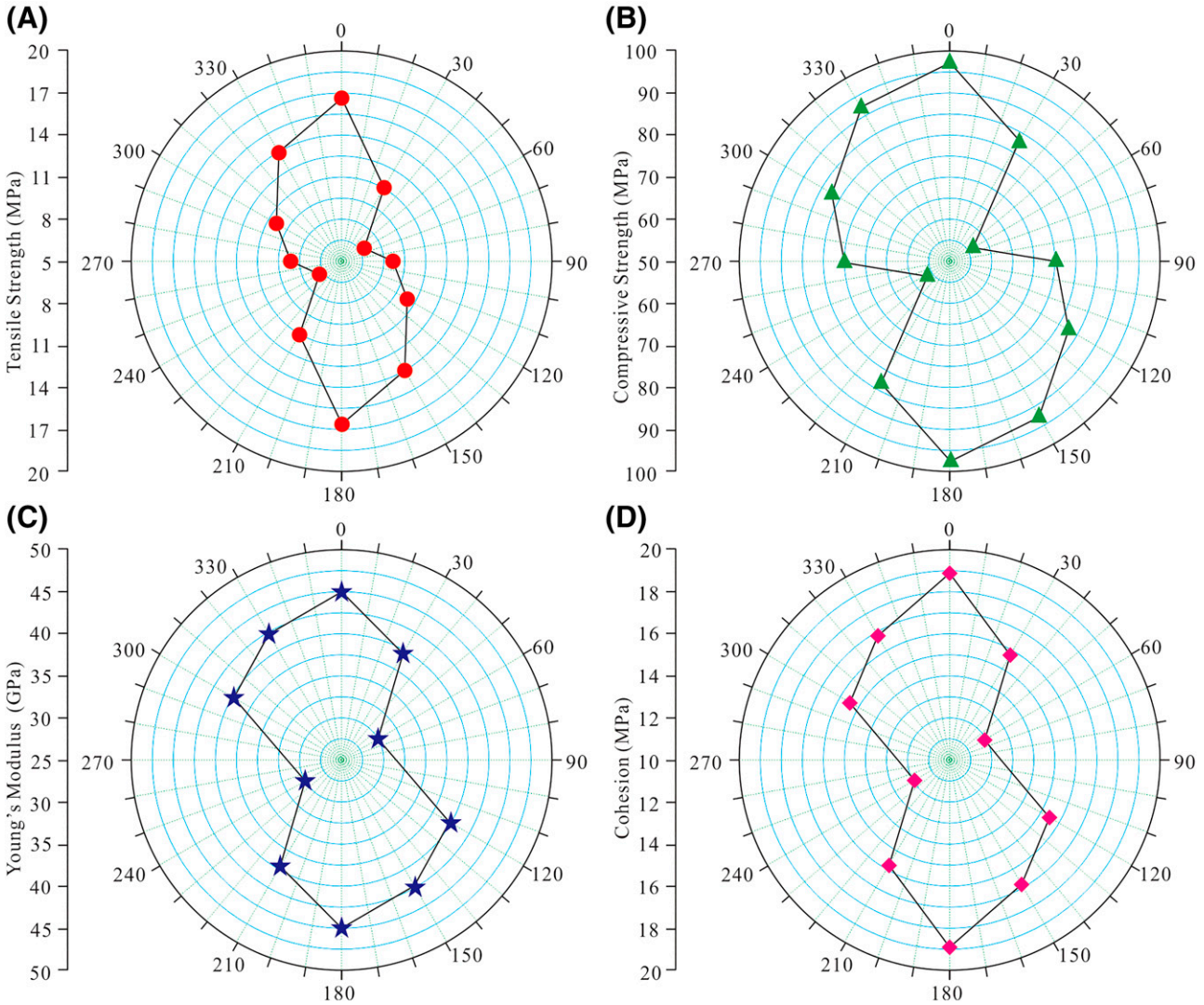


**Figure 16.** Difference of rock mechanical parameters in different directions of tight sandstones: (A) tensile strength difference; (B) compressive strength difference; (C) Young's modulus difference; and (D) cohesion difference. Modified from Gong et al. (2019b).

development and distribution in later stages. Early fractures confine the distribution of later fractures by controlling local stress, which can not only act as the expansion path of later fractures but also prevent the growth of later fractures. Therefore, transformation, restriction, and cutting occur among multistage fractures. Later fractures can cut early ones significantly when tectonic stress in the later stage is larger than that in the early stage, whereas early fractures can limit later fractures when the tectonic stress in the later stage is lower than that in the early stage (Zeng and Li, 2009; Gong et al., 2019c; Gao et al., 2020).

The extension direction of early fractures and its relationship with later maximum principal stress orientation can limit the superposition of two-phase fractures (Fossen, 2016; Gao et al., 2020). Deformation tests on fractured rock show that the tensile strength of the rock is the smallest when the angle between rocks and fracture surfaces is less than 30°, which is approximately 22%–28% of the rock with no fractures. Therefore, rock is easy to open along the existing fractures, and it is not easy to produce new fractures when the angle between the fracture surface and the minimum principal stress direction is less than 30°. The shearing strength of rock is the lowest when the angle between the fracture surface and principal compressive stress orientation is 15°–45°. Therefore, shear fractures easily occur along the early fractures when the angle between the fracture surface and the maximum principal stress

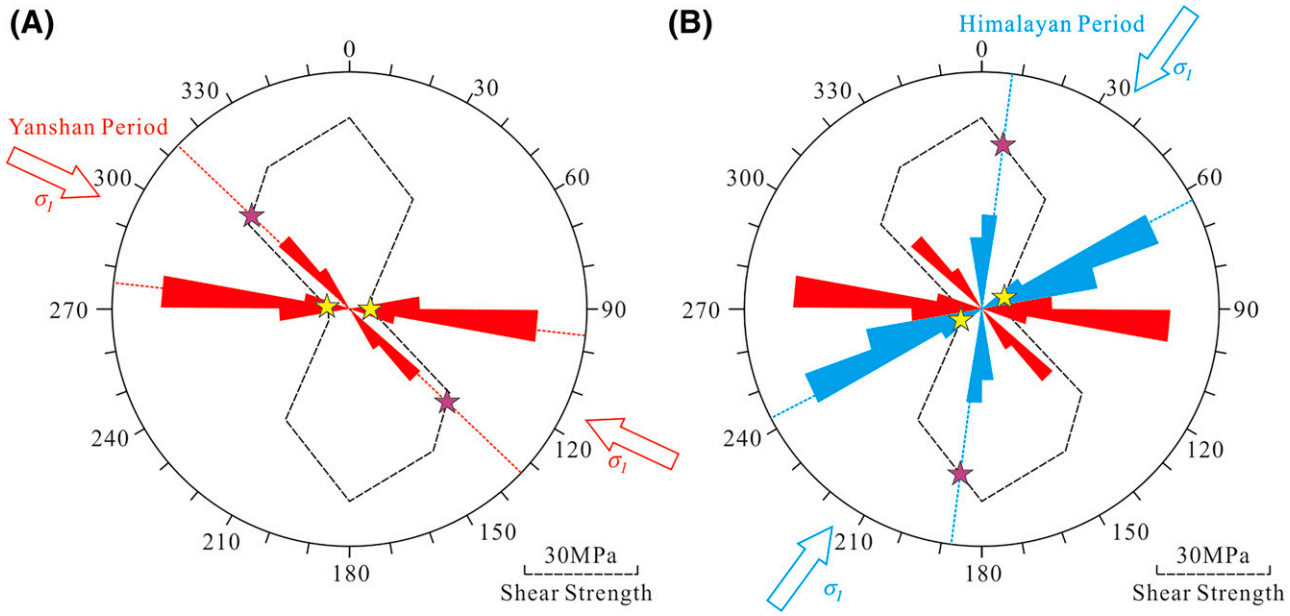


**Figure 17.** Influence of heterogeneity on fracture development in different directions. The black dotted line shows shear strength in different directions. (A) Northwest-southeast and near–east-west shear fractures can be theoretically formed under northwest-southeast compressive stress in the Yanshan period. However, the near–east-west fracture density is higher than the northwest-southeast fracture density because the northwest-southeast shearing strength (purple star) is larger than the near–east-west shearing strength (yellow stars). (B) Northeast-southwest and near–north-south shear fractures can be formed theoretically under the north-northeast–south-southwest tectonic compressive stress in the Himalayan period. However, the northeast-southwest fracture density is higher than that in the near–north-south direction because the near–north-south shearing strength (purple star) is higher than the northeast-southwest shearing strength (yellow stars).

orientation is 15°–45° (Zeng and Liu, 2010). New fractures can be generated when angles are out of this scope.

## Evolutionary Factors

Fracture growth in rocks is closely related to the stress state (Ferrill et al., 2021)—specifically, fracture occurrence is determined by three principal stress states. The fracture scale and intensity are controlled by the difference between maximum stress and minimum stress. Fracture occurrence and scale at different regional structures and buried depths vary greatly with stress states and amplitudes in different periods (see figure 4 in Ferrill et al., 2021).

The stress state in the crust can be expressed by vertical principal stress ($\sigma_V$), horizontal maximum principal stress ($\sigma_{Hmax}$), and horizontal minimum principal stress ($\sigma_{Hmin}$). Three stress regimes can be summarized based on the relationship among $\sigma_V$, $\sigma_{Hmax}$, and $\sigma_{Hmin}$: (1) normal faulting stress regime, $\sigma_V > \sigma_{Hmax} > \sigma_{Hmin}$; (2) strike-slip faulting regime, $\sigma_{Hmax} > \sigma_V > \sigma_{Hmin}$; and (3) thrust faulting stress regime, $\sigma_{Hmax} > \sigma_{Hmin} > \sigma_V$.

Overburden is the primary contributor to in situ stress during subsidence with no regional stress. Under this condition, the normal faulting stress regime occurs, where the maximum principal stress ($\sigma_1$) is the vertical principal stress ($\sigma_V$), and the minimum principal stress and intermediate principal stress are the horizontal ones ($\sigma_1 = \sigma_V > \sigma_2 = \sigma_{Hmax} > \sigma_3 = \sigma_{Hmin}$). Consequently, high-angle shear fractures (with an angle of 60°) and near-vertical tensile fractures can be produced.

Increasing horizontal compressive stress enables the horizontal maximum principal stress ($\sigma_{Hmax}$) to exceed the vertical principal stress ($\sigma_V$) ($\sigma_1 = \sigma_{Hmax} > \sigma_2 = \sigma_V > \sigma_3 = \sigma_{Hmin}$), where the maximum principal stress and the minimum principal stress can be horizontal and the intermediate principal stress is vertical, forming a strike-slip fault regime. Nearly vertical shear fractures and tensile fractures are mainly developed under this stress regime. Abnormal high pressure frequently occurring in tight sandstone reservoirs during deep burial and tectonic compression can result in tensile fractures (overpressure fractures) when pore fluid pressure exceeds the minimum principal stress.

Further increasing horizontal compressive stress or tectonic uplift can decrease the overlying stress, where the vertical principal stress ($\sigma_V$) can be converted to minimum principal stress ($\sigma_1 = \sigma_{Hmax} > \sigma_2 = \sigma_{Hmin} > \sigma_3 = \sigma_V$). As a result, the thrust faulting stress regime occurs, in which the maximum principal stress and the intermediate principal stress are horizontal and the minimum principal stress is vertical, generating low-angle shear fractures with a dip angle of approximately 30° and nearly horizontal tensile fractures.

The horizontal minimum principal stress will decrease with the horizontal compressive stress due to the Poisson effect. The strike-slip faulting regime exists when the horizontal minimum principal stress is reduced to the vertical principal stress ($\sigma_1 = \sigma_{Hmax} > \sigma_2 = \sigma_V > \sigma_3 = \sigma_{Hmin}$). The vertical principal stress becomes the maximum principal stress ($\sigma_1 = \sigma_V > \sigma_2 = \sigma_{Hmax} > \sigma_3 = \sigma_{Hmin}$) when horizontal compressive stress decreases further, giving rise to the normal faulting stress regime.

Paleostress is an important element determining fracture scale. Large tectonic stress is favorable for the development of large-scale fractures in rocks with obvious differences in mechanical properties and thickness between brittle layers and ductile layers. Small tectonic stress limits fracture expansion in rocks with small differences in mechanical properties and thickness between brittle layers and ductile layers, typically forming small-scale fractures. Therefore, medium-high angle throughgoing shear fractures and intralayer tensile fractures can be found in tight sandstone reservoirs in extensional tectonic environments (e.g., Bohai Bay Basin in eastern China). Nearly vertical throughgoing shear fractures and intralayer tensile fractures can be observed in tight sandstone reservoirs under weak compression environments with stable structures (e.g., Ordos Basin in China). Low-angle throughgoing shear fractures, bedding shear fractures, near-horizontal bedding fractures, and overpressure fractures are developed mainly in tight sandstone reservoirs under strong tectonic compression environments (e.g., Kuqa depression and Western Sichuan foreland basin in China).

## EFFECTIVE AND EVOLUTION OF NATURAL FRACTURES

The impact of natural fractures on tight sandstone reservoirs depends on their effectiveness and evolution. Effective fractures are open ones that can provide fluid storage space and fluid flow under confining pressures; otherwise, they are invalid fractures (Bons, 2000; Zeng et al., 2012b; Capezzuoli et al., 2018; Gong et al., 2021b; Liu et al., 2021b; Matera et al., 2021). Filling behavior in natural fractures can divide them into cement completely filled and partially filled or unfilled opening-mode fractures (Laubach, 2003; Laubach and Ward, 2006; Hooker et al., 2014; Ukar et al., 2019; Brogi et al., 2020). The fully filled veins are invalid fractures, whereas the partially filled or unfilled fractures are effective fractures. The effectiveness of natural fractures determines their contribution to tight sandstone reservoirs and their impact on well potential. Effective fractures can act as reservoir spaces and flow channels, whereas ineffective fractures hinder fluid flow and act as seepage barriers.

The fracture effectiveness is determined mainly by its growth period, cementation, dissolution, later tectonic movement, abnormally high-pressure fluid, in situ stress state, and so forth (Zeng et al., 2012a; Gong et al., 2015). The effectiveness of filled fractures in tight sandstone is controlled mainly by structural diagenesis (Laubach et al., 2010), especially the coupling of the fracture opening rate and the mineral filling rate (the ratio of filler width to filling time in fractures) (Gale et al., 2010). Fractures are completely filled with no effectiveness when their opening rate is lower than the mineral filling rate. Local filled and semifilled fractures are formed when the opening rate is higher than the filling rate (Figure 18), which can resist the closure of natural fractures and are insensitive to effective stress to keep opening and effectiveness (Laubach et al., 2004a; Gong et al., 2021b). Significant differences in filling behavior can be found in different parts of a single fracture (e.g., filling degree increases with decreasing fracture aperture, forming transition structures [mineral bridges]) (Laubach et al., 2004b). Fracture diagenesis—that is, mineral precipitation and dissolution in fractures and surrounding rocks—determines the filling rate and filling degree in fractures (Laubach, 2003). Comparison of fractures with different apertures suggests that fractures with a smaller aperture have a higher filling degree (Laubach et al., 2004b). Compared with shallow fractures, deep fractures with the same diagenesis background are seriously filled; this can be explained by the fact that fracture diagenesis in deep fractures is more active, resulting in a higher filling

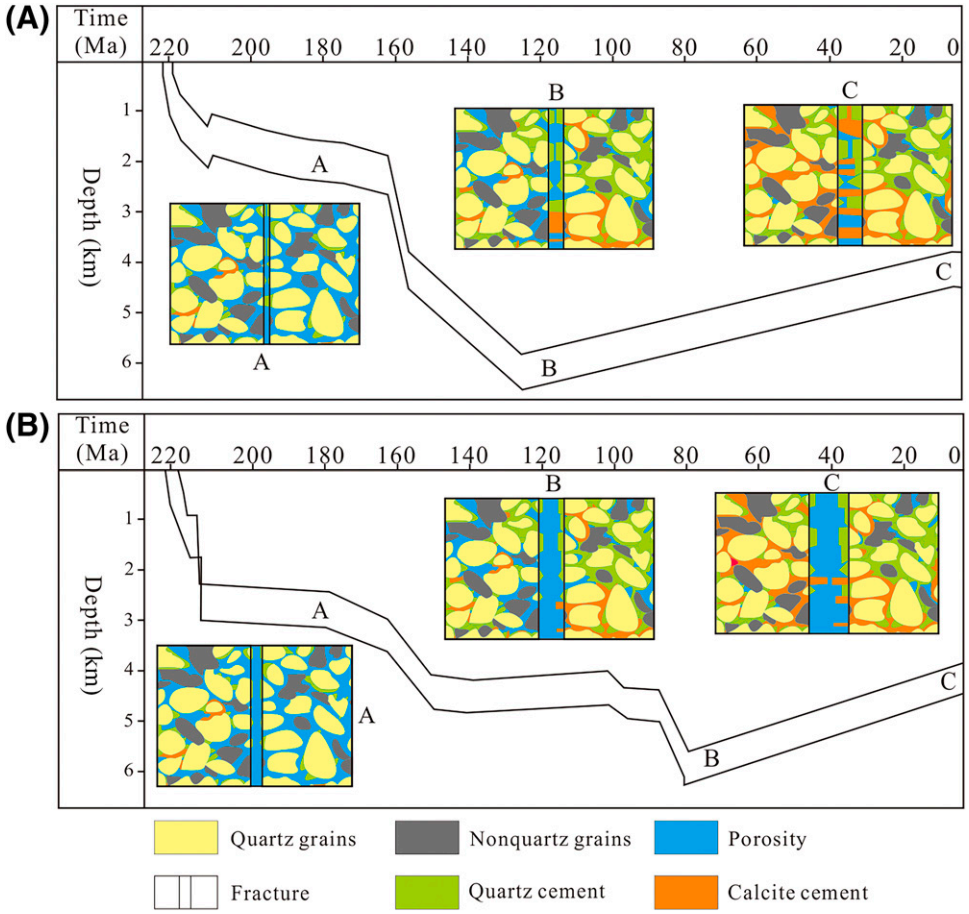


**Figure 18.** Evolution model of fracture effectiveness during burial of the Upper Triassic Xujiahe Formation in the western Sichuan Basin. (A) In the northern region, natural fractures present moderate effectiveness because the fracture opening rate was between the fastest growth rate (calcite) and the slowest growth rate (along quartz prismatic faces) under the weak tectonic activity. (B) In the southern region, natural fractures have good effectiveness since the fracture opening rate outstripped the fastest growth rate (calcite) influenced by the strong tectonic activity.

rate (Laubach et al., 2019). Fractures are frequently filled with quartz in siliceous-cemented rocks (Ellis et al., 2012), whereas they are generally filled with calcite in calcite-cemented rocks. Fractures cemented by quartz are often semifilled, where authigenic quartz hangs on fracture walls or connects two fracture walls as a bridge, leaving considerable pores in fractures. Fillings (e.g., calcite, gypsum, other minerals) are often in a block or fiber shape. The earlier fractures are more seriously filled compared to later fractures (Laubach and Diaz-Tushman, 2011; Zeng et al., 2012b). Fillings in fractures can be dissolved in a later stage to form dissolution pores along fractures, increasing fracture effectiveness. Abnormal high pressure and late tectonic uplift can open the early filled fractures and also improve fracture effectiveness (Zeng et al., 2012b).

The effectiveness of unfilled fractures in tight sandstone is controlled by fracture apertures and closely related to in situ stress. Fractures have large apertures, high permeability, and good connectivity and effectiveness when they are nearly parallel to the current principal stress, whereas they have small apertures, low permeability, and poor connectivity and effectiveness when they are nearly perpendicular to the current principal stress due to the large normal stress perpendicular to the fracture surface (Zeng and Li, 2009). Natural fractures parallel to the current principal stress are usually the main seepage in tight sandstone, which is the basis of the well pattern principle for tight sandstone reservoirs. For semifilled fractures, filled minerals (mineral bridges) can support and keep fractures open, even if the fractures are not parallel to the current maximum principal stress,

which can be used as an important seepage channel (Laubach et al., 2004a). Fracture effectiveness varies with dip angles—that is, high-angle fractures are more effective than the low-angle fractures.

## FRACTURE PREDICTION

Quantitative prediction of natural fracture distribution is always a challenging task. At present, the existing natural fracture prediction methods mainly include structural curvature (Murray, 1968; Jamison, 2016); fractal (Ortega et al., 2006; Gong et al., 2019c); paleotectonic stress field numerical simulation (Gao et al., 2015); strain energy (Ding et al., 1998); conventional and image logs (Zeng et al., 2013; Lyu et al., 2016; Dong et al., 2020a–c); and geophysical methods (e.g., poststack coherence, curvature, likelihood, prestack amplitude variation with azimuth) (Lohr et al., 2008; Fernández-Ibáñez et al., 2018; Boersma et al., 2020; Wang et al., 2022). However, due to the large burial depth and relatively low seismic resolution of tight sandstone reservoirs in China, it is difficult to identify natural fractures by geophysical methods. At the same time, the rock mechanics properties of tight sandstone reservoirs have strong anisotropy, which makes the fracture development degree of different directions significantly different. We propose a quantitative prediction method for natural fractures based on the fracture density of single wells, rock mechanical parameters of different lithologies or lithofacies and the magnitude and orientation of the stress field. A geological model is established in this paper based on the above geological factors. The numerical simulation of the paleotectonic stress field during fracture growth is performed to quantitatively predict structural fracture distribution in tight sandstone reservoirs based on rock fracture criteria, in which fracture data from cores are used as constraints.

### Numerical Simulation of Paleotectonic Stress Field during Fracture Growth

Natural fracture development in tight sandstone can be predicted by reservoir geomechanics based on its origin, evolution, and control factors (Gao et al., 2015; Gong et al., 2019b). Fracture genesis and characteristics can be identified based on qualitative and quantitative characterizations of multiscale natural fractures from outcrops, imaging log, cores, and thin sections. Primary controlling elements of the fracture growth period, effective evolution, and distribution are determined based on acoustic emission, fracture filling, fluid inclusion, and structural evolution history (Gong et al., 2019a). Finally, a heterogeneous geological model is established based on elements controlling fracture distribution (e.g., lithology, sedimentary microfacies, diagenetic facies, faults, and fluid pressure).

Rock mechanics parameters (elastic modulus, Poisson's ratio, cohesion, tensile strength, and internal friction angle) of various lithofacies are given based on rock mechanics tests on different lithofacies samples. After that, geomechanical simulation is performed using the finite element method to describe paleotectonic stress fields during fracture growth, where the continuous elastic geological body is divided into finite elements. These elements are connected by nodes, and displacements on these nodes are obtained using equilibrium conditions, which can be used to determine the strain and stress of these elements. Increasing units and decreasing their size can tend to truly express complex geological bodies.

### Determination of Fracture Occurrence

Fracture type and occurrence in rock can be determined using measured rock mechanics parameters and calculated principal stress magnitude and orientation, in which the Griffith failure criterion is used to identify whether tensile fractures can occur and their occurrence (Camac and Hunt, 2009; Bons et al., 2012; Fossen, 2016). The orientation of potential tensile fracture surface is determined using the angle ($\alpha$) between it and maximum principal stress when $\sigma_1 + 3\sigma_3 \geq 0$ (here, the stress is positive in compression and negative in tension):

$$cos\alpha = \frac{(\sigma_1 - \sigma_3)}{2(\sigma_1 + \sigma_3)} \tag{2}$$

The tensile stress on this potential tensile fracture surface is

$$\sigma_t = \frac{(\sigma_1 - \sigma_3)^2}{8(\sigma_1 + \sigma_3)} \tag{3}$$

Tensile fractures can be generated when $\sigma_t \geq [\sigma_t]$, $[\sigma_t]$ is tensile strength in the normal direction of the potential tensile fracture surface.

The potential tensile fracture surface is perpendicular to the minimum principal stress $\sigma_3$ when $\sigma_1 + 3\sigma_3 \le 0$, and the tensile strength on this surface is

$$\sigma_t = -\sigma_3 \tag{4}$$

The Mohr-Coulomb failure criterion can be used to identify whether shear fractures can occur and their occurrence (Maerten et al., 2006; Lohr et al., 2008; Camac and Hunt, 2009; Bons et al., 2012). The angle ($\theta$) between shear fractures and the maximum principal stress can be expressed as

$$\theta = 45^\circ - \frac{\varphi}{2} \tag{5}$$

where $\theta$ is the shearing angle and $\varphi$ is the internal friction angle. The shear strength of the potential shear fracture surface is

$$[\tau] = C + \sigma_N tg\varphi \tag{6}$$

where $[\tau]$ is the potential shear fracture surface, C is cohesion, $\sigma_N$ is the normal stress on the potential shear fracture surface, and $\varphi$ is the internal friction angle. Shear fractures can be produced when the shear strength on the potential shear fracture surface is $\tau \ge [\tau]$.

## Fracture Density Prediction

The fracture index ($I$) can quantitatively describe fracture development in rock (Ding et al., 1998; Gong et al., 2019b), which is defined as the ratio of shear stress or tensile stress in one unit to the actual shear or tensile strength of rock. It can be expressed as

$$I = \frac{\tau_n}{[\tau_n]} \text{ or } I = \frac{\sigma_t}{[\sigma_t]} \tag{7}$$

where $\tau_n$ and $\sigma_t$ are shear stress and tensile stress, respectively; $[\tau_n]$ and $[\sigma_t]$ are shear strength and tensile strength, respectively; $I < 1$ indicates that rocks are not fractured; and $I \ge 1$ represents fracture occurrence in rocks. The fracture index value represents the possibility of fracture development in rocks.

Fracture behavior in rocks suggests that whether fractures can be produced in rocks depends on the fracturing rate of rocks, whereas the fracture scale is related to the energy accumulated in rocks. Comparison of fractures from cores shows that the fracture density has a good correlation with fracturing rate and strain energy. Therefore, these two parameters can be used to predict fracture density (Ding et al., 1998). The strain energy can be calculated by the following expression:

$$W = \frac{1}{2E}[\sigma_1^2 + \sigma_2^2 + \sigma_3^2 - 2\nu(\sigma_1\sigma_2 + \sigma_1\sigma_3 + \sigma_2\sigma_3)] \tag{8}$$

where $W$ is the strain energy, $E$ is the elastic modulus, $\nu$ is Poisson's ratio, $\sigma_1$ is the maximum principal stress, $\sigma_2$ is the intermediate principal stress, and $\sigma_3$ is the minimum principal stress.

The fracture density from cores can be fitted with fracturing rate and strain energy calculated from a simulated stress field using the least-squares method, and the fitting formula can be used to calculate fracture distribution (Ding et al., 1998). The fracture density can be expressed using rock strain energy and fracturing rate as follows:

$$\rho = A_1 I_r^2 + A_2 W^2 + A_3 I_r + A_4 W + A_5 \ (I_r \ge I_0) \tag{9}$$

$$\rho = A_1 I_r^2 + A_2 I_r + A_3 \ (I_r < I_0) \tag{10}$$

where $\rho$ is the predicted fracture density, $I_r$ is the comprehensive fracturing rate acquired from the standardized tensile fracture rate and the shear fracture rate, and $W$ is rock strain energy; $A_1$, $A_2$, $A_3$, $A_4$, and $A_5$ are undetermined coefficients, respectively, and $I_0$ is the critical value of the comprehensive fracturing rate.

Rock mechanical property anisotropy controls fracture intensity in different directions. Therefore, rock mechanical parameter measurement should be performed not only on different lithofacies but also on different directions of the same lithofacies, where fracture intensity in different directions can be calculated.

## Jiyuan Oilfield Case Study

Jiyuan oilfield is located in the west of the Ordos Basin, China. The fourth and fifth members of the Upper Triassic Yanchang Formation are typical tight sandstone reservoirs. Taking the tight sandstone reservoir as an example, we quantitatively predicted its fracture distribution using the above method.

The geological model is the basis and premise of the whole numerical simulation, which directly

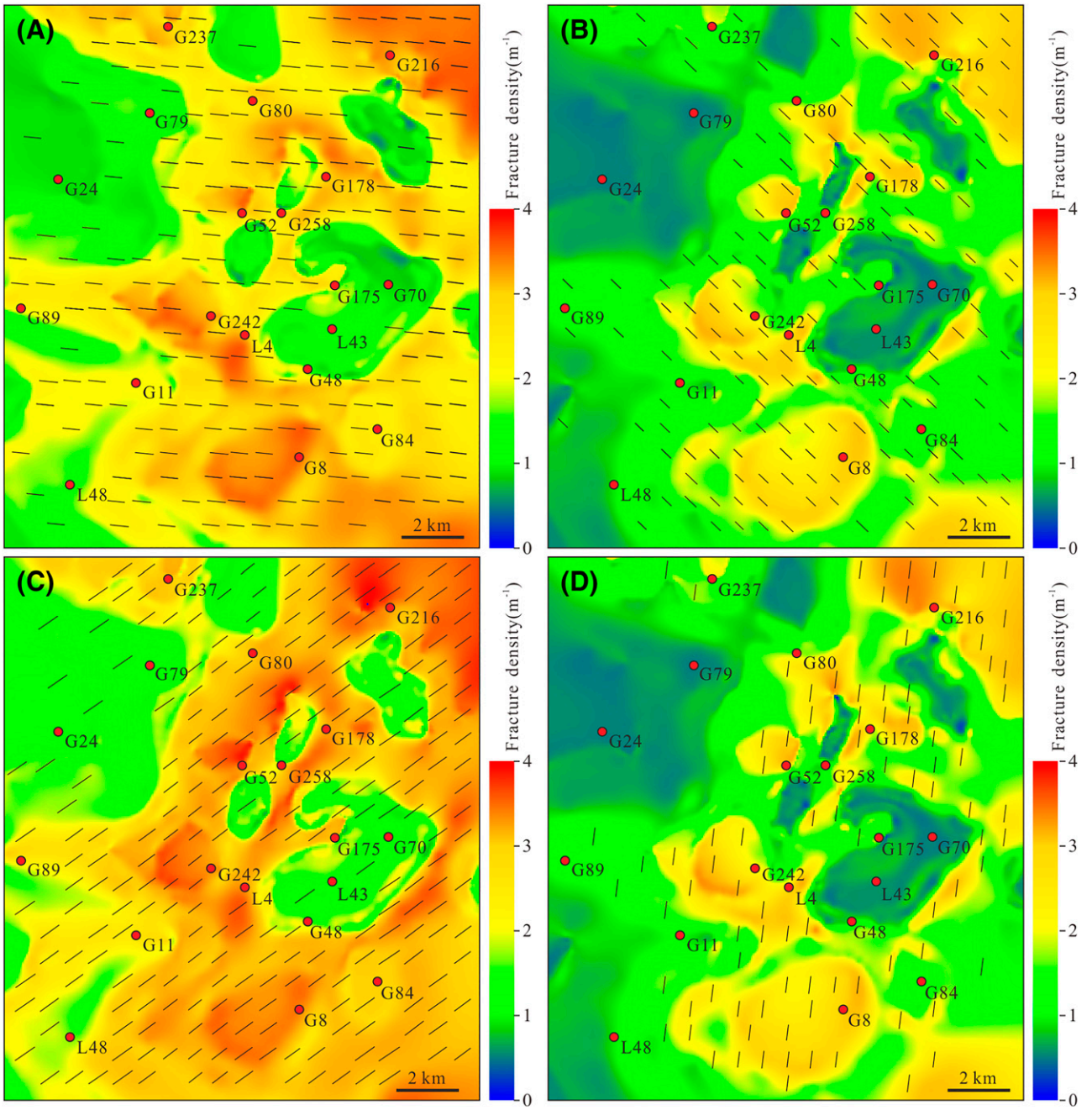


**Figure 19.** Predicted fracture distribution at the fourth and fifth members of the Upper Triassic Yanchang Formation in the Jiyuan Area, Ordos Basin. The short lines represent the fracture strike. (A–D) The density distribution of four sets of fractures. Modified from Gong et al. (2019b). The red dots represent well locations.

determines the reasonable selection of the mechanical model. The fractures formed mainly at the end of the Jurassic and the end of the Cretaceous in this area (Gong et al., 2019b), so the paleotectonic maps of the Jurassic and Cretaceous were selected as geological models. The main factors affecting the fracture development in the study area include lithology, bed thickness, and sedimentary microfacies, and the sedimentary microfacies contain the information regarding lithology and bed thickness to a certain extent. Therefore, the sedimentary microfacies map in the study area is used to reflect the plane heterogeneity of the reservoir.

To study the differences in the mechanical properties of rock in different directions and their influence on fracture development, uniaxial and triaxial

**Table 4.** Comparison between Measured and Predicted Fracture Density

| Well Name | Fracture Density | | Absolute Error | Relative Error, % |
|---|---|---|---|---|
| | Measured | Predicted | | |
| G175 | 1.21 $m^{-1}$ (0.369 $ft^{-1}$) | 1.40 $m^{-1}$ (0.427 $ft^{-1}$) | −0.19 $m^{-1}$ (−0.058 $ft^{-1}$) | 14.07 |
| G178 | 1.21 $m^{-1}$ (0.369 $ft^{-1}$) | 1.23 $m^{-1}$ (0.375 $ft^{-1}$) | −0.02 $m^{-1}$ (−0.006 $ft^{-1}$) | 1.73 |
| G237 | 1.96 $m^{-1}$ (0.597 $ft^{-1}$) | 2.06 $m^{-1}$ (0.628 $ft^{-1}$) | −0.10 $m^{-1}$ (−0.030 $ft^{-1}$) | 5.17 |
| G242 | 3.65 $m^{-1}$ (1.113 $ft^{-1}$) | 4.25 $m^{-1}$ (1.295 $ft^{-1}$) | −0.60 $m^{-1}$ (−0.183 $ft^{-1}$) | 13.96 |
| G258 | 0.70 $m^{-1}$ (0.213 $ft^{-1}$) | 0.83 $m^{-1}$ (0.253 $ft^{-1}$) | −0.13 $m^{-1}$ (−0.040 $ft^{-1}$) | 16.23 |
| G48 | 0.30 $m^{-1}$ (0.091 $ft^{-1}$) | 0.36 $m^{-1}$ (0.110 $ft^{-1}$) | −0.06 $m^{-1}$ (−0.018 $ft^{-1}$) | 15.97 |
| G52 | 3.26 $m^{-1}$ (0.994 $ft^{-1}$) | 2.67 $m^{-1}$ (0.814 $ft^{-1}$) | 0.59 $m^{-1}$ (0.180 $ft^{-1}$) | 15.42 |
| G70 | 0.10 $m^{-1}$ (0.030 $ft^{-1}$) | 0.11 $m^{-1}$ (0.034 $ft^{-1}$) | −0.01 $m^{-1}$ (−0.003 $ft^{-1}$) | 9.78 |
| G79 | 0.08 $m^{-1}$ (0.024 $ft^{-1}$) | 0.10 $m^{-1}$ (0.030 $ft^{-1}$) | −0.02 $m^{-1}$ (−0.006 $ft^{-1}$) | 16.06 |
| G8 | 2.81 $m^{-1}$ (0.856 $ft^{-1}$) | 3.18 $m^{-1}$ (0.969 $ft^{-1}$) | −0.37 $m^{-1}$ (−0.113 $ft^{-1}$) | 11.66 |
| G80 | 0.65 $m^{-1}$ (0.198 $ft^{-1}$) | 0.55 $m^{-1}$ (0.168 $ft^{-1}$) | 0.10 $m^{-1}$ (0.030 $ft^{-1}$) | 17.16 |
| G84 | 0.21 $m^{-1}$ (0.064 $ft^{-1}$) | 0.22 $m^{-1}$ (0.067 $ft^{-1}$) | −0.01 $m^{-1}$ (−0.003 $ft^{-1}$) | 5.51 |
| G89 | 0.18 $m^{-1}$ (0.055 $ft^{-1}$) | 0.17 $m^{-1}$ (0.052 $ft^{-1}$) | 0.01 $m^{-1}$ (0.003 $ft^{-1}$) | 2.54 |
| L4 | 1.38 $m^{-1}$ (0.421 $ft^{-1}$) | 1.18 $m^{-1}$ (0.360 $ft^{-1}$) | 0.19 $m^{-1}$ (0.058 $ft^{-1}$) | 16.35 |
| L43 | 0.30 $m^{-1}$ (0.091 $ft^{-1}$) | 0.25 $m^{-1}$ (0.076 $ft^{-1}$) | 0.05 $m^{-1}$ (0.015 $ft^{-1}$) | 19.18 |

Modified from Gong et al. (2019b).

rock mechanics experiments were carried out on rock samples in different directions (Figure 16). The tensile strength of rock is measured directly by the splitting tensile test. Young's modulus, Poisson's ratio, cohesion, and the internal friction angle were obtained by triaxial rock mechanical experiments.

According to the characteristics of fracture formation in two stages, the paleotectonic stress field of two stages is numerically simulated (Figure 17). According to the comprehensive analysis of the azimuth and magnitude of the principal stress obtained from the study of the tectonic stress field and acoustic emission test (Gong et al., 2019b), the initial boundary conditions are set as follows in the numerical simulation: The first stage is affected mainly by the near-horizontal compression stress of west-northwest–east-southeast (295°∠3°), with the maximum principal stress of 105 MPa and the minimum principal stress of 20 MPa; the second stage is the near-horizontal compression stress of north-northeast–south-southwest (35°∠2°); the maximum principal stress is approximately 85 MPa and the minimum principal stress is approximately 10 MPa.

In accordance with the above geological model, rock mechanical parameters, and boundary conditions, the ANSYS18 finite element software was used to numerically simulate the paleotectonic stress field of the two stages. Then, according to the difference in rock mechanical properties in different directions, the Griffith failure criterion and the Mohr-Coulomb shear fracture criterion were used to calculate the fracture rates of different directions in different stages of the study area. Finally, the fracture index and strain energy were fitted with the fracture density of a single well, and the distribution of fracture density was predicted.

Figure 19 shows the predicted natural fracture direction and density in the Upper Triassic Yanchang tight sandstone reservoir in the Jiyuan oilfield. Results show that the study area is dominated by shear fractures. Four sets of high-angle shear fractures are predicted under two-stage compressive stress, namely, the east-west fractures (Figure 19A) and the northwest-southeast fractures (Figure 19B) of the first stage and the northeast-southwest fractures (Figure 19C) and the north-south fractures (Figure 19D) of the second stage, the orientation of which is consistent with that interpreted from the imaging log (Figure 17).

Rock mechanical property anisotropy results in different fracture densities of two groups of conjugate shear fractures developing in the same period, in which the northeast-southwest fractures and the east-west fractures are the most common in the studied area, with average linear densities of 2.91 $m^{-1}$ (0.89 $ft^{-1}$) and 2.74 $m^{-1}$ (0.84 $ft^{-1}$), respectively.

The north-south fractures and the northwest-southeast fractures are weakly developed, with a linear density generally less than 1.5 $m^{-1}$ (0.46 $ft^{-1}$), whereas high fracture density (2.0 $m^{-1}$ [0.61 $ft^{-1}$]) occurs only in individual areas.

We analyzed the reliability of the prediction results using fracture data from 19 well image logs and 15 well core data logs (Table 4). The results show that the strike errors of the four sets are 6.03°, −2.39°, 0.64°, and −4.68° and that the dip angle errors are 5.3°, 4.7°, 7.7°, and 5.0°, respectively. The predicted fracture development degree is consistent with the statistical results of the core fracture density. Among them, the error of 5 wells is less than 10% and the error of the other 10 wells is between 10% and 20%, with an average of 12.05%, indicating that the predicted results are highly reliable.

## CONCLUSION

1. Four types of natural fractures can be identified in tight sandstone reservoirs (e.g., tectonic fractures, diagenetic fractures, tectonic-diagenetic fractures, overpressure fractures). The structural fractures are the most important. Structural fractures can be further divided into intralayer open fractures, throughgoing shear fractures, and bedding shear fractures based on the mechanical properties of structural fractures and their spatial coupling with the bedding plane. Diagenetic fractures are commonly bedding fractures. Tectonic-diagenetic fractures are mainly intragranular fractures and grain-edge fractures formed by tectonic compression and compaction. Overpressure fractures are lenticular tension fractures filled with minerals.
2. Natural fractures are multiscale, which can be divided into four levels: large scale, medium scale, small scale, and microscale based on their size and associated mechanical interface. Fractures of different sizes are controlled by corresponding mechanical interfaces. The formation and distribution of multiscale natural fractures are controlled by three main elements: paleotectonic stress, mechanical stratigraphic property difference, and ductile layer thickness. Large tectonic stress and small differences in the mechanical property and thickness between the brittle layer and the ductile layer are favorable for large-scale fracture growth, whereas small tectonic stress and large differences in the mechanical property and thickness contribute to small-scale fracture development. Different-scale fractures distribute in a power trend with few large fractures but considerable small fractures. Large- and medium-scale fractures work mainly as seepage channels; small-scale fractures can be seepage channels and reservoirs, whereas microscale fractures act as reservoirs.
3. Natural fractures are heterogeneously distributed laterally and vertically due to the control of internal factors, dynamic factors, heterogeneity, and evolution. Internal factors (lithology, mechanical stratigraphy, sedimentary microfacies, and diagenetic facies) determine the deformation pattern of tight sandstone reservoirs and fracture development in different positions. The local stress concentration caused by dynamic factors (structural location and pore fluid pressure) enhances the heterogeneity of fracture distribution. Heterogeneity (lateral rock mechanic anisotropy and existing fractures) affects fracture development and its size in different directions. The paleotectonic stress determines the fracture type and occurrence. The paleotectonic stress magnitude, mechanical layer property differences, and ductile layer thickness work together to control the scales of natural fractures.
4. Fracture effectiveness varies with its formation period, cementation, dissolution, later tectonism, abnormally high-pressure fluid, and in situ stress state. Fully filled veins are ineffective fractures and partially filled or unfilled fractures are effective fractures. The high-angle unfilled fractures parallel to the current maximum principal stress are higher in aperture, permeability, and effectiveness compared with those in other directions. Aperture and effectiveness of partially filled fractures have little to do with the current stress orientation because of the support derived from fillings.
5. A fracture distribution prediction method based on fracture-influencing factors and geomechanical simulation was presented in this paper. First, using image logs, cores, and thin section data, the multiscale fracture system was characterized and the main controlling factors of fracture distribution were identified. Second, a geological

model was established based on the spatial distribution characteristics of these controlling factors, such as sedimentary microfacies, the formation pressure coefficient, the sand:mud ratio, faults, and so forth. Through rock mechanics experiments, the corresponding rock mechanical parameters were assigned to the geological model at different positions, and the magnitude and direction of regional paleotectonic stress during the fracture formation period were taken as boundary conditions to conduct the numerical simulation of the stress field. Third, the distribution of fractures in different directions of tight sandstone reservoirs can be calculated and quantitatively predicted by combining the fracture criteria obtained from rock mechanics tests in different lithofacies and different directions and the fine characterization results of fractures in different scales. The predicted fracture development degree is in agreement with the statistical results of fracture density in single wells.

## REFERENCES CITED


Aguilera, R., 1980, Naturally fractured reservoirs: Tulsa, Oklahoma, PennWell Books, 703 p.

Almansour, A., S. E. Laubach, J. E. Bickel, and R. A. Schultz, 2020, Value of information analysis of a fracture prediction method: SPE Reservoir Evaluation & Engineering, v. 23, no. 3, p. 811–823, doi:10.2118/198906-PA.

Ameen, M. S., K. MacPherson, M. I. Al-Marhoon, and Z. Rahim, 2012, Diverse fracture properties and their impact on performance in conventional and tight-gas reservoirs, Saudi Arabia: The Unayzah, South Haradh case study: AAPG Bulletin, v. 96, no. 3, p. 459–492, doi:10.1306/06011110148.

Awdal, A., R. Suramairy, K. Singh, G. Fabre, and G. I. Alsop, 2020, Deformation bands and their impact on fluid flow: Insights from geometrical modelling and multi-scale flow simulations in sandstones: Journal of Structural Geology, v. 141, 104215, 19 p., doi:10.1016/j.jsg.2020.104215.

Bai, T., and D. D. Pollard, 2000, Fracture spacing in layered rocks: A new explanation based on the stress transition: Journal of Structural Geology, v. 22, no. 1, p. 43–57, doi:10.1016/S0191-8141(99)00137-6.

Bertotti, G., N. Hardebol, J. K. Taal-van Koppen, and S. M. Luthi, 2007, Toward a quantitative definition of mechanical units: New techniques and results from an outcropping deep-water turbidite succession (Tanqua-Karoo Basin, South Africa): AAPG Bulletin, v. 91, no. 8, p. 1085–1098, doi:10.1306/03060706074.

Boersma, Q., W. Athmer, M. Haege, M. Etchebes, J. Haukås, and G. Bertotti, 2020, Natural fault and fracture network characterization for the southern Ekofisk field: A case study integrating seismic attribute analysis with image log interpretation: Journal of Structural Geology, v. 141, 104197, 14 p., doi:10.1016/j.jsg.2020.104197.

Bons, P. D., 2000, The formation of veins and their microstructures: Journal of the Virtual Explorer, v. 2, 3 p., doi:10.3809/jvirtex.2000.00007.

Bons, P. D., M. A. Elburg, and E. Gomez-Rivas, 2012, A review of the formation of tectonic veins and their microstructures: Journal of Structural Geology, v. 43, p. 33–62, doi:10.1016/j.jsg.2012.07.005.

Braathen, A., E. Petrie, T. Nystuen, A. Sundal, E. Skurtveit, V. Zuchuat, M. Gutierrez, and I. Midtkandal, 2020, Interaction of deformation bands and fractures during progressive strain in monocline; San Rafael Swell, central Utah, USA: Journal of Structural Geology, v. 141, p. 104219, doi:10.1016/j.jsg.2020.104219.

Brogi, A., 2011, Variation in fracture patterns in damage zones related to strike-slip faults interfering with pre-existing fractures in sandstone (Calcione area, southern Tuscany, Italy): Journal of Structural Geology, v. 33, no. 4, p. 644–661, doi:10.1016/j.jsg.2010.12.008.

Brogi, A., M. C. Alçiçek, D. Liotta, E. Capezzuoli, M. Zucchi, and P. F. Matera, 2021, Step-over fault zones controlling geothermal fluid-flow and travertine formation: (Denizli Basin, Turkey): Geothermics, v. 89, 101941, 17 p., doi:10.1016/j.geothermics.2020.101941.

Brogi, A., M. C. Alçiçek, C. C. Yalciner, E. Capezzuoli, D. Liotta, M. Meccheri, V. Rimondi, G. Ruggieri, A. Gandin, and C. Boschi, 2016, Hydrothermal fluids circulation and travertine deposition in an active tectonic setting: Insights from the Kamara geothermal area: Tectonophysics, v. 680, no. 1, p. 211–232, doi:10.1016/j.tecto.2016.05.003.

Brogi, A., D. Liotta, E. Capezzuoli, P. Matera, S. Kele, M. Soligo, P. Tuccimei, et al., 2020, Travertine deposits constraining transfer zone neotectonics in geothermal areas: An example from the inner northern Apennines (Bagno Vignoni-Val d'Orcia area, Italy): Geothermics, v. 85, 101763, 22 p., doi:10.1016/j.geothermics.2019.101763.

Camac, B. A., and S. P. Hunt, 2009, Predicting the regional distribution of fracture networks using the distinct element numerical method: AAPG Bulletin, v. 93, no. 11, p. 1571–1583, doi:10.1306/07230909040.

Capezzuoli, E., G. Ruggieri, V. Rimondi, A. Brogi, D. Liotta, M. C. Alçiçek, H. Alçiçek, et al., 2018, Calcite veining and feeding conduits in a hydrothermal system: Insights from a natural section across the Pleistocene Gölemezli travertine depositional system (western Anatolia, Turkey): Journal of Structural Geology, v. 364, p. 180–203, doi:10.1016/j.sedgeo.2017.12.012.

Cawood, A. J., C. E. Bond, J. A. Howell, R. W. H. Butler, and Y. Totake, 2017, LiDAR, UAV or compass-clinometer? Accuracy, coverage and the effects on structural models: Journal of Structural Geology, v. 98, p. 67–82, doi:10.1016/j.jsg.2017.04.004.

Chang, X., J. Wang, C. Tang, and Z. Ru, 2016, Effects of interface behavior on fracture spacing in layered rock: Rock Mechanics and Rock Engineering, v. 49, no. 5, p. 1733–1746, doi:10.1007/s00603-015-0852-5.

Chang, X., H. Zhao, and L. Cheng, 2020, Fracture propagation and coalescence at bedding plane in layered rocks: Journal of Structural Geology, v. 141, 104213, 15 p., doi:10.1016/j.jsg.2020.104213.

Choi, J., P. Edwards, K. Ko, and Y. Kim, 2016, Definition and classification of fault damage zones; A review and a new methodological approach: Earth-Science Reviews, v. 152, p. 70–87, doi:10.1016/j.earscirev.2015.11.006.

Corradetti, A., S. Tavani, M. Parente, A. Iannace, F. Vinci, C. Pirmez, S. Torrieri, M. Giorgioni, A. Pignalosa, and S. Mazzoli, 2018, Distribution and arrest of vertical through-going joints in a seismic-scale carbonate platform exposure (Sorrento peninsula, Italy): Insights from integrating field survey and digital outcrop model: Journal of Structural Geology, v. 108, p. 121–136, doi:10.1016/j.jsg.2017.09.009.

Cox, S. F., 2010, The application of failure mode diagrams for exploring the roles of fluid pressure and stress states in controlling styles of fracture-controlled permeability enhancement in faults and shear zones: Geofluids, v. 10, no. 1–2, p. 217–233, doi:10.1111/j.1468-8123.2010.00281.x.

Cumella, S., and J. Scheevel, 2012, Mesaverde tight gas sandstone sourcing from underlying Mancos-Niobrara shales: AAPG Search and Discovery article 10450, accessed July 26, 2023, https://www.searchanddiscovery.com/documents/2012/10450cumella/ndx_cumella.pdf.

Ding, Z., X. Qian, H. Huo, and Y. Yang, 1998, A new method for quantitative prediction of tectonic fractures-Two factor method [in Chinese with English abstract]: Oil & Gas Geology, v. 19, no. 1, p. 3–9.

Dong, S., L. Zeng, J. Liu, A. Gao, W. Lyu, X. Du, K. Yang, and M. Bao, 2020a, Fracture identification in tight reservoirs by multiple kernel Fisher discriminant analysis using conventional logs: Interpretation, v. 8, no. 4, p. SP215–SP225, doi:10.1190/INT-2020-0048.1.

Dong, S., L. Zeng, W. Lyu, D. Xia, G. Liu, Y. Wu, and X. Du, 2020b, Fracture identification and evaluation using conventional logs in tight sandstones: A case study in the Ordos Basin, China: Energy Geoscience, v. 1, no. 3–4, p. 115–123, doi: 10.1016/j.engeos.2020.06.003.

Dong, S., L. Zeng, W. Lyu, C. Xu, J. Liu, Z. Mao, H. Tian, and F. Sun, 2020c, Fracture identification by semi-supervised learning using conventional logs in tight sandstones of Ordos Basin, China: Journal of Natural Gas Science and Engineering, v. 76, 103131, 11 p., doi:10.1016/j.jngse.2019.103131.

Dutton, S. P., S. J. Clift, D. S. Hamilton, H. S. Hamlin, T. F. Hentz, W. E. Howard, M. S. Akhter, and S. E. Laubach, 1993, Major low-permeability sandstone gas reservoirs in the continental United States: Austin, Texas, The University of Texas at Austin Bureau of Economic Geology Report of Investigations 211, 221 p., accessed August 11, 2023, https://www.beg.utexas.edu/publications/major-low-permeability-sandstone-gas-reservoirs-continental-united-states.

Dutton, S. P., and T. N. Diggs, 1992, Evolution of porosity and permeability in the Lower Cretaceous Travis Peak Formation, East Texas: AAPG Bulletin, v. 76, no. 2, p. 252–269, doi:10.1306/BDFF87C2-1718-11D7-8645000102C1865D.

Dutton, S. P., and R. J. Finley, 1988, Controls on reservoir quality in tight sandstones of the Travis Peak Formation, East Texas: SPE Formation Evaluation, v. 3, no. 1, p. 97–104, doi:10.2118/15220-PA.

Ellis, M. A., S. E. Laubach, P. Eichhubl, J. E. Olson, and P. Hargrove, 2012, Fracture development and diagenesis of Torridon Group Applecross Formation, near An Teallach, NW Scotland: Millennia of brittle deformation resilience?: Journal of the Geological Society, v. 169, no. 3, p. 297–310, doi:10.1144/0016-76492011-086.

Faulkner, D. R., C. A. L. Jackson, R. J. Lunn, R. W. Schlische, Z. K. Shipton, C. A. J. Wibberley, M. O. Withjack, et al., 2010, A review of recent developments concerning the structure, mechanics and fluid flow properties of fault zones: Journal of Structural Geology, v. 32, no. 11, p. 1557–1575, doi:10.1016/j.jsg.2010.06.009.

Fernández-Ibáñez, F., J. M. DeGraff, and F. Ibrayev, 2018, Integrating borehole image logs with core: A method to enhance subsurface fracture characterization: AAPG Bulletin, v. 102, no. 6, p. 1067–1090, doi:10.1306/0726171609317002.

Ferrill, D. A., R. N. McGinnis, A. P. Morris, K. J. Smart, Z. T. Sickman, M. Bentz, D. Lehrmann, and M. A. Evans, 2014, Control of mechanical stratigraphy on bed-restricted jointing and normal faulting: Eagle Ford Formation, south-central Texas: AAPG Bulletin, v. 98, no. 11, p. 2477–2506, doi:10.1306/08191414053.

Ferrill, D. A., A. P. Morris, R. N. McGinnis, K. J. Smart, S. S. Wigginton, and N. J. Hill, 2017, Mechanical stratigraphy and normal faulting: Journal of Structural Geology, v. 94, p. 275–302, doi:10.1016/j.jsg.2016.11.010.

Ferrill, D. A., K. J. Smart, A. J. Cawood, and A. P. Morris, 2021, The fold-thrust belt stress cycle: Superposition of normal, strike-slip, and thrust faulting deformation regimes: Journal of Structural Geology, v. 148, 104362, 12 p., doi:10.1016/j.jsg.2021.104362.

Forbes Inskip, N. D., J. Browning, P. G. Meredith, and A. Gudmundsson, 2020, Conditions for fracture arrest in layered rock sequences: Results in Geophysical Sciences, v. 1–4, 100001, 11 p., doi:10.1016/j.ringps.2020.100001.

Fossen, H., 2010, Deformation bands formed during soft-sediment deformation; Observations from SE Utah: Marine and Petroleum Geology, v. 27, no. 1, p. 215–222, doi:10.1016/j.marpetgeo.2009.06.005.

Fossen, H., 2016, Structural geology, 2nd ed.: Cambridge, United Kingdom, Cambridge University Press, 510 p., doi:10.1017/9781107415096.

Fossen, H., and A. Bale, 2007, Deformation bands and their influence on fluid flow: AAPG Bulletin, v. 91, no. 12, p. 1685–1700, doi:10.1306/07300706146.

Fossen, H., R. A. Schultz, and A. Torabi, 2011, Conditions and implications for compaction band formation in the Navajo Sandstone, Utah: Journal of Structural

Geology, v. 33, no. 10, p. 1477–1490, doi:10.1016/j.jsg.2011.08.001.

Fu, Y., and H. Dehghanpour, 2020, How far can hydraulic fractures go? A comparative analysis of water flowback, tracer, and microseismic data from the Horn River Basin: Marine and Petroleum Geology, v. 115, 104259, 10 p., doi:10.1016/j.marpetgeo.2020.104259.

Gale, J. F. W., R. H. Lander, R. M. Reed, and S. E. Laubach, 2010, Modeling fracture porosity evolution in dolostone: Journal of Structural Geology, v. 32, no. 9, p. 1201–1211, doi:10.1016/j.jsg.2009.04.018.

Gale, J. F. W., S. E. Laubach, J. E. Olson, P. Eichhuble, and A. Fall, 2014, Natural fractures in shale: A review and new observations: AAPG Bulletin, v. 98, no. 11, p. 2165–2216, doi:10.1306/08121413151.

Gao, S., S. Chen, H. Pu, L. Gong, S. Ma, Q. Luo, X. Wang, A. Gao, and B. Zhang, 2019, Fine characterization of large composite channel sandbody architecture and its control on remaining oil distribution: A case study of alkaline-surfactant-polymer (ASP) flooding test area in Xingshugang oilfield, China: Journal of Petroleum Science Engineering, v. 175, p. 363–374, doi:10.1016/j.petrol.2018.12.033.

Gao, S., L. Gong, X. Liu, B. Liu, A. Gao, X. Su, J. Wang, and J. Li, 2020, Distribution and controlling factors of natural fractures in deep tight volcanic gas reservoirs in Xujiaweizi area, Northern Songliao Basin: [in Chinese with English abstract]: Oil & Gas Geology, v. 41, no. 3, p. 503–512, doi:10.11743/ogg20200307.

Gao, S., L. Zeng, S. Ma, Y. He, L. Gong, X. Zhao, W. Xu, and X. Zhao, 2015, Quantitative prediction of fractures with different directions in tight sandstone reservoir: [in Chinese with English abstract]: Natural Gas Geoscience, v. 26, no. 3, p. 427–434.

Gong, L., X. Fu, Z. Wang, S. Gao, H. Jabbari, W. Yue, and B. Liu, 2019a, A new approach for characterization and prediction of natural fracture occurrence in tight oil sandstones with intense anisotropy: AAPG Bulletin, v. 103, no. 6, p. 1383–1400, doi:10.1306/12131818054.

Gong, L., M. Gao, L. Zeng, X. Fu, Z. Gao, A. Gao, K. Zu, and J. Yao, 2017a, Factors on fracture development in the tight sandstone reservoirs: A case study of Jurassic-Neogene in the Kuqa foreland basin [in Chinese with English abstract]: Natural Gas Geoscience, v. 28, no. 2, p. 199–208.

Gong, L., S. Gao, X. Fu, S. Chen, B. Lyu, and J. Yao, 2017b, Fracture characteristics and their effects on hydrocarbon migration and accumulation in tight volcanic reservoirs: A case study of the Xujiaweizi fault depression, Songliao Basin, China: Interpretation, v. 5, no. 4, p. SP57–SP70, doi:https://doi.org/10.1190/INT-2016-0227.1.

Gong, L., S. Gao, B. Liu, J. Yang, X. Fu, F. Xiao, X. Su, R. Fu, and Q. Lu, 2021a, Quantitative prediction of natural fractures in shale oil reservoirs: Geofluids, v. 2021, 5571855, 15 p., doi:10.1155/2021/5571855.

Gong, L., B. Liu, X. Fu, H. Jabbari, S. Gao, W. Yue, H. Yuan, R. Fu, and Z. Wang, 2019b, Quantitative prediction of sub-seismic faults and their impact on waterflood performance: Bozhong 34 oilfield case study: Journal of Petroleum Science Engineering, v. 172, p. 60–69, doi:10.1016/j.petrol.2018.09.049.

Gong, L., K. Q. Liu, and W. Ju, 2023, Editorial: Advances in the study of natural fractures in deep and unconventional reservoirs: Frontiers of Earth Science, v. 10, 1096643, 3 p., doi:10.3389/feart.2022.1096643.

Gong, L., X. Su, S. Gao, X. Fu, H. Jabbari, X. Wang, B. Liu, W. Yue, Z. Wang, and A. Gao, 2019c, Characteristics and formation mechanism of natural fractures in the tight gas sandstones of Jiulongshan gas field, China: Journal of Petroleum Science Engineering, v. 175, p. 1112–1121, doi:10.1016/j.petrol.2019.01.021.

Gong, L., J. Wang, S. Gao, X. Fu, B. Liu, F. Miao, X. Zhou, and Q. Meng, 2021b, Characterization, controlling factors and evolution of fracture effectiveness in shale oil reservoirs: Journal of Petroleum Science Engineering, v. 203, p. 108655, doi:10.1016/j.petrol.2021.108655.

Gong, L., J. Yao, S. Gao, B. Wei, L. Zeng, X. Fu, Z. Gao, K. Zu, and H. Tian, 2018, Controls of rock mechanical stratigraphy on tectonic fracture spacing [in Chinese with English abstract]: Geotectonica et Metallogenia, v. 42, no. 6, p. 965–973, doi:10.16539/j.ddgzyckx.2018.06.002.

Gong, L., L. Zeng, Y. Du, and Z. Hang, 2015, Influences of structural diagenesis on fracture effectiveness: A case study of the Cretaceous tight sandstone reservoirs of Kuqa foreland basin [in Chinese with English abstract]: Journal of China University of Mining and Technology, v. 44, no. 3, p. 514–519, doi:10.13247/j.cnki.jcumt.000263.

Gong, L., L. Zeng, Z. Gao, R. Zhu, and B. Zhang, 2016, Reservoir characterization and origin of tight gas sandstones in the Upper Triassic Xujiahe formation, western Sichuan Basin, China: Journal of Petroleum Exploration and Production Technology, v. 6, no. 3, p. 319–329, doi:10.1007/s13202-015-0203-9.

Gross, M. R., and Y. Eyal, 2007, Throughgoing fractures in layered carbonate rocks: Geological Society of America Bulletin, v. 119, no. 11–12, p. 1387–1404, doi:10.1130/0016-7606(2007)119[1387:TFILCR]2.0.CO;2.

Gross, M. R., M. P. Fischer, T. Engelder, and R. J. Greenfield, 1995, Factors controlling joint spacing in interbedded sedimentary rocks: Integrating numerical models with field observations from the Monterey Formation, USA, *in* M. S. Ameen, ed., Fractography: Fracture topography as a tool in fracture mechanics and stress analysis: Geological Society, London, Special Publications 1995, v. 92, p. 215–233, doi:10.1144/GSL.SP.1995.092.01.12.

Gudmundsson, A., 1999, Fluid overpressure and stress drop in fault zones: Geophysical Research Letters, v. 26, no. 1, p. 115–118, doi:10.1029/1998GL900228.

Hansberry, R. L., R. C. King, S. P. Holford, M. Hand, and N. Debenham, 2021, How wide is a fault damage zone? Using network topology to examine how fault-damage zones overprint regional fracture networks: Journal of Structural Geology, v. 146, 104327, 9 p., doi:10.1016/j.jsg.2021.104327.

Healy, D., R. E. Rizzo, D. G. Cornwell, N. J. C. Farrell, H. Watkins, N. E. Timms, E. Gomez-Rivas, and M. Smith,

2017, FracPaQ: A MATLAB$^{TM}$ toolbox for the quantification of fracture patterns: Journal of Structural Geology, v. 95, p. 1–16, doi:10.1016/j.jsg.2016.12.003.

Helgeson, D. E., and A. Aydin, 1991, Characteristics of joint propagation across layer interfaces in sedimentary rocks: Journal of Structural Geology, v. 13, no. 8, p. 897–911, doi:10.1016/0191-8141(91)90085-W.

Hooker, J. N., S. E. Laubach, and R. Marrett, 2013, Fracture-aperture size—Frequency, spatial distribution, and growth processes in strata-bounded and non-strata-bounded fractures, Cambrian Mesón Group, NW Argentina: Journal of Structural Geology, v. 54, p. 54–71, doi:10.1016/j.jsg.2013.06.011.

Hooker, J. N., S. E. Laubach, and R. Marrett, 2014, A universal power-law scaling exponent for fracture apertures in sandstones: GSA Bulletin, v. 126, no. 9–10, p. 1340–1362, doi:10.1130/B30945.1.

Hooker, J. N., S. E. Laubach, and R. Marrett, 2018, Microfracture spacing distributions and the evolution of fracture patterns in sandstones: Journal of Structural Geology, v. 108, p. 66–79, doi:10.1016/j.jsg.2017.04.001.

Howard, J. H., 1990, Description of natural fracture systems for quantitative use in petroleum geology: AAPG Bulletin, v. 74, no. 2, p. 151–162, doi:10.1306/0C9B2281-1710-11D7-8645000102C1865D.

Hu, T., X. Pang, F. Jiang, Q. Wang, X. Liu, Z. Wang, S. Jiang, et al., 2021, Movable oil content evaluation of lacustrine organic-rich shales: Methods and a novel quantitative evaluation model: Earth-Science Reviews, v. 214, 103545, 26 p., doi:10.1016/j.earscirev.2021.103545.

Jamison, W., 2016, Fracture system evolution within the Cardium sandstone, central Alberta Foothills folds: AAPG Bulletin, v. 100, no. 7, p. 1099–1134, doi:10.1306/03011515082.

Johri, M., M. D. Zoback, and P. Hennings, 2014, A scaling law to characterize fault-damage zones at reservoir depths: AAPG Bulletin, v. 98, no. 10, p. 2057–2079, doi:10.1306/05061413173.

Kim, Y., D. C. P. Peacock, and D. J. Sanderson, 2004, Fault damage zones: Journal of Structural Geology, v. 26, no. 3, p. 503–517, doi:10.1016/j.jsg.2003.08.002.

Kim, Y., and D. J. Sanderson, 2005, The relationship between displacement and length of faults: A review: Earth-Science Reviews, v. 68, no. 3–4, p. 317–334, doi:10.1016/j.earscirev.2004.06.003.

Kranz, R. L., 1983, Microcracks rocks. A review: Tectonophysics, v. 100, no. 1–3, p. 449–480, doi:10.1016/0040-1951(83)90198-1.

Lai, J., G. Wang, S. Wang, J. Cao, M. Li, X. Pang, Z. Zhou, et al., 2018a, Review of diagenetic facies in tight sandstones: Diagenesis, diagenetic minerals, and prediction via well logs: Earth-Science Reviews, v. 185, p. 234–258, doi:10.1016/j.earscirev.2018.06.009.

Lai, J., G. Wang, Z. Wang, J. Chen, X. Pang, S. Wang, Z. Zhou, Z. He, Z. Qin, and X. Fan, 2018b, A review on pore structure characterization in tight sandstones: Earth-Science Reviews, v. 177, p. 436–457, doi:10.1016/j.earscirev.2017.12.003.

Lamarche, J., A. P. C. Lavenu, B. D. M. Gauthier, Y. Guglielmi, and O. Jayet, 2012, Relationships between fracture patterns, geodynamics and mechanical stratigraphy in Carbonates (South-East Basin, France): Tectonophysics, v. 581, p. 231–245, doi:10.1016/j.tecto.2012.06.042.

Lao, H., Y. Wang, N. Meng, and Z. Wu, 2021, Architectural characteristics and evolution sequences of different types of faults in extensional basins—Evidence collected from cores in the Dongying Depression: Marine and Petroleum Geology, v. 132, 105199, 17 p., doi:10.1016/j.marpetgeo.2021.105199.

Larsen, B., and A. Gudmundsson, 2010, Linking of fractures in layered rocks: Implications for permeability: Tectonophysics, v. 492, no. 1–4, p. 108–120, doi:10.1016/j.tecto.2010.05.022.

Larsen, B., A. Gudmundsson, I. Grunnaleite, G. Saelen, M. R. Talbot, and S. J. Buckley, 2010, Effects of sedimentary interfaces on fracture pattern, linkage, and cluster formation in peritidal carbonate rocks: Marine and Petroleum Geology, v. 27, no. 7, p. 1531–1550, doi:10.1016/j.marpetgeo.2010.03.011.

Laubach, S. E., 1997, A method to detect natural fracture strike in sandstones: AAPG Bulletin, v. 81, no. 4, p. 604–623, doi:10.1306/522B43E3-1727-11D7-8645000102C1865D.

Laubach, S. E., 2003, Practical approaches to identifying sealed and open fractures: AAPG Bulletin, v. 87, no. 4, p. 561–579, doi:10.1306/11060201106.

Laubach, S. E., and K. Diaz-Tushman, 2011, Laurentian palaeostress trajectories and ephemeral fracture permeability, Cambrian Eriboll Formation sandstones west of the Moine Thrust Zone, NW Scotland: Journal of the Geological Society, v. 166, no. 2, p. 349–362, doi:10.1144/0016-76492008-061.

Laubach, S. E., P. Eichhubl, C. Hilgers, and R. H. Lander, 2010, Structural diagenesis: Journal of Structural Geology, v. 32, no. 12, p. 1866–1872, doi:10.1016/j.jsg.2010.10.001.

Laubach, S. E., A. Fall, L. K. Copley, R. Marrett, and S. J. Wilkins, 2016, Fracture porosity creation and persistence in a basement-involved Laramide fold, Upper Cretaceous Frontier Formation, Green River Basin, USA: Geological Magazine, v. 153, no. 5–6, p. 887–910, doi:10.1017/S0016756816000157.

Laubach, S. E., R. H. Lander, L. J. Criscenti, L. M. Anovitz, J. L. Urai, R. M. Pollyea, J. N. Hooker, et al., 2019, The role of chemistry in fracture pattern development and opportunities to advance interpretations of geological materials: Reviews of Geophysics, v. 57, no. 3, p. 1065–1111, doi:10.1029/2019RG000671.

Laubach, S. E., J. E. Olson, and J. F. W. Gale, 2004a, Are open fractures necessarily aligned with maximum horizontal stress?: Earth and Planetary Science Letters, v. 222, no. 1, p. 191–195, doi:10.1016/j.epsl.2004.02.019.

Laubach, S. E., R. M. Reed, J. E. Olson, R. H. Lander, and L. M. Bonnell, 2004b, Coevolution of crack-seal texture and fracture porosity in sedimentary rocks: Cathodoluminescence observations of regional fractures: Journal of

Structural Geology, v. 26, no. 5, p. 967–982, doi:10.1016/j.jsg.2003.08.019.

Laubach, S. E., and M. E. Ward, 2006, Diagenesis in porosity evolution of opening-mode fractures, Middle Triassic to Lower Jurassic La Boca Formation, NE Mexico: Tectonophysics, v. 419, no. 1–4, p. 75–97, doi:10.1016/j.tecto.2006.03.020.

Lavenu, A. P. C., and J. Lamarche, 2018, What controls diffuse fractures in platform carbonates? Insights from Provence (France) and Apulia (Italy): Journal of Structural Geology, v. 108, p. 94–107, doi:10.1016/j.jsg.2017.05.011.

Lee, H. P., J. E. Olson, and R. A. Schultz, 2018, Interaction analysis of propagating opening mode fractures with veins using the discrete element method: International Journal of Rock Mechanics and Mining Sciences, v. 103, p. 275–288, doi:10.1016/j.ijrmms.2018.01.005.

Liu, B., S. He, L. Meng, X. Fu, L. Gong, and H. Wang, 2021a, Sealing mechanisms in volcanic faulted reservoirs in Xujiaweizi extension, northern Songliao Basin, northeastern China: AAPG Bulletin, v. 105, no. 8, p. 1721–1743, doi:10.1306/03122119048.

Liu, G., L. Zeng, X. Wang, M. Ostadhassan, Z. Wang, Z. Mao, and Q. Tie, 2020, Natural fractures in deep tight gas sandstone reservoirs in the thrust belt of the southern Junggar Basin, northwestern China: Interpretation, v. 8, no. 4, p. SP81–SP93, doi:10.1190/INT-2020-0051.1.

Liu, G., L. Zeng, R. Zhu, L. Gong, M. Ostadhassan, and Z. Mao, 2021b, Effective fractures and their contribution to the reservoirs in deep tight sandstones in the Kuqa Depression, Tarim Basin, China: Marine and Petroleum Geology, v. 124, 104824, 15 p., doi:10.1016/j.marpetgeo.2020.104824.

Lohr, T., C. M. Krawczyk, D. C. Tanner, R. Samiee, H. Endres, P. O. Thierer, O. Oncken, H. Trappe, R. Bachmann, and P. A. Kukla, 2008, Prediction of subseismic faults and fractures: Integration of three-dimensional seismic data, three-dimensional retrodeformation, and well data on an example of deformation around an inverted fault: AAPG Bulletin, v. 92, no. 4, p. 473–485, doi:10.1306/11260707046.

Lorenz, J. C., J. L. Sterling, D. S. Schechter, C. L. Whigham, and J. L. Jensen, 2002, Natural fractures in the Spraberry Formation, Midland Basin, Texas: The effects of mechanical stratigraphy on fracture variability and reservoir behavior: AAPG Bulletin, v. 86, no. 3, p. 505–524, doi:10.1306/61EEDB20-173E-11D7-8645000102C1865D.

Lorenz, J. C., L. W. Teufel, and N. R. Warpinski, 1991, Regional fractures I: A mechanism for the formation of regional fractures at depth in flat-lying reservoirs: AAPG Bulletin, v. 75, no. 11, p. 1714–1737, doi:10.1306/0C9B29E3-1710-11D7-8645000102C1865D.

Lorenz, J. C., N. R. Warpinski, L. W. Teufel, P. T. Branagan, A. R. Sattler, and D. A. Northrop, 1988, Results of the multiwell experiment in situ stresses, natural fractures, and other geological controls on reservoirs: Eos, v. 69, no. 35, p. 817–826, doi:10.1029/88EO01079.

Luo, Q., L. Gong, Y. Qu, K. Zhang, G. Zhang, and S. Wang, 2018, The tight oil potential of the Lucaogou Formation from the southern Junggar Basin, China: Fuel, v. 234, p. 858–871, doi:10.1016/j.fuel.2018.07.002.

Lyu, W., L. Zeng, S. Chen, P. Lyu, S. Dong, C. Hui, R. Li, and H. Wang, 2021, Characterization methods of multiscale natural fractures in tight and low-permeability sandstone reservoirs [in Chinese with English abstract]: Dizhi Lunping, v. 67, no. 2, p. 543–556, doi:10.16509/j.georeview.2021.02.020.

Lyu, W., L. Zeng, Z. Liu, G. Liu, and K. Zu, 2016, Fracture responses of conventional logs in tight-oil sandstones: A case study of the Upper Triassic Yanchang Formation in southwest Ordos Basin, China: AAPG Bulletin, v. 100, no. 9, p. 1399–1417, doi:10.1306/04041615129.

Lyu, W., L. Zeng, P. Lyu, T. Yi, S. Dong, S. Wang, X. Xu, and H. Chen, 2022, Insights into the mechanical stratigraphy and vertical fracture patterns in tight oil sandstones: The Upper Triassic Yanchang Formation in the eastern Ordos Basin, China: Journal of Petroleum Science Engineering, v. 212, 110247, 18 p., doi:10.1016/j.petrol.2022.110247.

Lyu, W., L. Zeng, B. Zhang, F. Miao, P. Lyu, and S. Dong, 2017, Influence of natural fractures on gas accumulation in the Upper Triassic tight gas sandstones in the northwestern Sichuan Basin, China: Marine and Petroleum Geology, v. 83, p. 60–72, doi:10.1016/j.marpetgeo.2017.03.004.

Lyu, W., L. Zeng, S. Zhou, X. Du, D. Xia, G. Liu, J. Li, and J. Weng, 2019, Natural fractures in tight-oil sandstones: A case study of the Upper Triassic Yanchang Formation in the southwestern Ordos Basin, China: AAPG Bulletin, v. 103, no. 10, p. 2343–2367, doi:10.1306/0130191608617115.

Maerten, L., P. Gillespie, and J. Daniel, 2006, Three-dimensional geomechanical modeling for constraint of subseismic fault simulation: AAPG Bulletin, v. 90, no. 9, p. 1337–1358, doi:10.1306/03130605148.

Mao, Z., L. Zeng, G. Liu, G. Liu, H. Tian, S. Dong, W. Lyu, and M. Ostadhassan, 2022, Controls of fault-bend fold on natural fractures: Insight from discrete element simulation and outcrops in the southern margin of the Junggar Basin, Western China: Marine and Petroleum Geology, v. 138, 105541, 15 p., doi:10.1016/j.marpetgeo.2022.105541.

Matera, P. F., G. Ventruti, M. Zucchi, A. Brogi, E. Capezzuoli, D. Liotta, T. Yu, et al., 2021, Geothermal fluid variation recorded by banded Ca-carbonate veins in a fault-related, fissure ridge-type travertine depositional system (Iano, southern Tuscany, Italy): Geofluids, v. 2021, 8817487, 28 p., doi:10.1155/2021/8817487.

McGinnis, R. N., D. A. Ferrill, A. P. Morris, K. J. Smart, and D. Lehrmann, 2017, Mechanical stratigraphic controls on natural fracture spacing and penetration: Journal of Structural Geology, v. 95, p. 160–170, doi:10.1016/j.jsg.2017.01.001.

Mi, L., H. Fan, T. Fan, L. Gong, T. Niu, X. Su, J. Luo, and Y. Sun, 2023, Development characteristics of multi-scale fracture network systems in metamorphic buried hills: Frontiers of Earth Science, v. 10, 1108032, 12 p., doi:10.3389/feart.2022.1108032.

Miranda, T. S., R. F. Santos, J. A. Barbosa, I. F. Gomes, M. L. Alencar, O. J. Correia, T. C. Falcão, J. F. W. Gale, and V. H. Neumann, 2018, Quantifying aperture, spacing and fracture intensity in a carbonate reservoir analogue: Crato Formation, NE Brazil: Marine and Petroleum Geology, v. 97, p. 556–567, doi:10.1016/j.marpetgeo.2018.07.019.

Murray, G. H., 1968, Quantitative fracture study, Sanish pool, Mckenzie County, North Dakota: AAPG Bulletin, v. 52, no. 1, p. 57–65, doi:10.1306/5D25C293-16C1-11D7-8645000102C1865D.

Narr, W., 1991, Fracture density in the deep subsurface: Techniques with application to Point Arguello oil field: AAPG Bulletin, v. 75, no. 8, p. 1300–1323, doi:10.1306/0C9B2939-1710-11D7-8645000102C1865D.

Narr, W., and I. Lerche, 1984, A method for estimating subsurface fracture density in core: AAPG Bulletin, v. 68, no. 5, p. 637–648, doi:10.1306/AD461354-16F7-11D7-8645000102C1865D.

Narr, W., and J. Suppe, 1991, Joint spacing in sedimentary rocks: Journal of Structural Geology, v. 13, no. 9, p. 1037–1048, doi:10.1016/0191-8141(91)90055-N.

Odling, N. E., 1997, Scaling and connectivity of joint systems in sandstones from western Norway: Journal of Structural Geology, v. 19, no. 10, p. 1257–1271, doi:10.1016/S0191-8141(97)00041-2.

Ogata, K., F. Storti, F. Balsamo, R. Tinterri, E. Bedogni, M. Fetter, L. Gomes, and R. Hatushika, 2016, Sedimentary facies control on mechanical and fracture stratigraphy in turbidites: GSA Bulletin, v. 129, no. 1–2, p. 76–92, doi:10.1130/B31517.1.

Olson, J. E., S. E. Laubach, and R. H. Lander, 2009, Natural fracture characterization in tight gas sandstones: Integrating mechanics and diagenesis: AAPG Bulletin, v. 93, no. 11, p. 1535–1549, doi:10.1306/08110909100.

Ortega, O. J., R. A. Marrett, and S. E. Laubach, 2006, A scale-independent approach to fracture intensity and average spacing measurement: AAPG Bulletin, v. 90, no. 2, p. 193–208, doi:10.1306/08250505059.

Ozkan, A., S. P. Cumella, K. L. Milliken, and S. E. Laubach, 2011, Prediction of lithofacies and reservoir quality using well logs, Late Cretaceous Williams Fork Formation, Mamm Creek Field, Piceance Basin, Colorado: AAPG Bulletin, v. 95, no. 10, p. 1699–1723, doi:10.1306/01191109143.

Peacock, D. C. P., C. W. Nixon, A. Rotevatn, D. J. Sanderson, and L. F. Zuluaga, 2016, Glossary of fault and other fracture networks: Journal of Structural Geology, v. 92, p. 12–29, doi:10.1016/j.jsg.2016.09.008.

Petrie, E. S., J. P. Evans, and S. J. Bauer, 2014, Failure of caprock seals as determined from mechanical stratigraphy, stress history, and tensile-failure analysis of exhumed analogs: AAPG Bulletin, v. 98, no. 11, p. 2365–2389, doi:10.1306/06171413126.

Philit, S., R. Soliva, R. Castilla, G. Ballas, and A. Taillefer, 2018, Clusters of cataclastic deformation bands in porous sandstones: Journal of Structural Geology, v. 114, p. 235–250, doi:10.1016/j.jsg.2018.04.013.

Pollard, D. D., and A. Aydin, 1988, Progress in understanding jointing over the past century: GSA Bulletin, v. 100, no. 8, p. 1181–1204, doi:10.1130/0016-7606(1988)100<1181:PIUJOT>2.3.CO;2.

Rodrigues, R. D. S., F. C. Alves Da Silva, and V. C. Córdoba, 2021, Evolution of deformation bands, insights from structural diagenesis: Journal of Structural Geology, v. 143, 104257, 11 p., doi:10.1016/j.jsg.2020.104257.

Rotevatn, A., and H. Fossen, 2011, Simulating the effect of subseismic fault tails and process zones in a siliciclastic reservoir analogue: Implications for aquifer support and trap definition: Marine and Petroleum Geology, v. 28, no. 9, p. 1648–1662, doi:10.1016/j.marpetgeo.2011.07.005.

Sanderson, D. J., and C. W. Nixon, 2015, The use of topology in fracture network characterization: Journal of Structural Geology, v. 72, p. 55–66, doi:10.1016/j.jsg.2015.01.005.

Sanderson, D. J., and C. W. Nixon, 2018, Topology, connectivity and percolation in fracture networks: Journal of Structural Geology, v. 115, p. 167–177, doi:10.1016/j.jsg.2018.07.011.

Sanderson, D. J., and D. C. P. Peacock, 2019, Line sampling of fracture swarms and corridors: Journal of Structural Geology, v. 122, p. 27–37, doi:10.1016/j.jsg.2019.02.006.

Smart, K. J., G. I. Ofoegbu, A. P. Morris, R. N. McGinnis, and D. A. Ferrill, 2014, Geomechanical modeling of hydraulic fracturing: Why mechanical stratigraphy, stress state, and pre-existing structure matter: AAPG Bulletin, v. 98, no. 11, p. 2237–2261, doi:10.1306/07071413118.

Strijker, G., G. Bertotti, and S. M. Luthi, 2012, Multi-scale fracture network analysis from an outcrop analogue: A case study from the Cambro-Ordovician clastic succession in Petra, Jordan: Marine and Petroleum Geology, v. 38, no. 1, p. 104–116, doi:10.1016/j.marpetgeo.2012.07.003.

Tongwa, P., R. Nygaard, A. Blue, and B. Bai, 2013, Evaluation of potential fracture-sealing materials for remediating $CO_2$ leakage pathways during $CO_2$ sequestration: International Journal of Greenhouse Gas Control, v. 18, p. 128–138, doi:10.1016/j.ijggc.2013.06.017.

Torabi, A., and S. S. Berg, 2011, Scaling of fault attributes: A review: Marine and Petroleum Geology, v. 28, no. 8, p. 1444–1460, doi:10.1016/j.marpetgeo.2011.04.003.

Ukar, E., S. E. Laubach, and J. N. Hooker, 2019, Outcrops as guides to subsurface natural fractures: Example from the Nikanassin Formation tight-gas sandstone, Grande Cache, Alberta foothills, Canada: Marine and Petroleum Geology, v. 103, p. 255–275, doi:10.1016/j.marpetgeo.2019.01.039.

Underwood, C. A., M. L. Cooke, J. A. Simo, and M. A. Muldoon, 2003, Stratigraphic controls on vertical fracture patterns in Siarian dolomite, northeastern Wisconsin: AAPG Bulletin, v. 87, no. 1, p. 121–142.

Wang, K., R. Zhang, J. Wang, X. Sun, and X. Yang, 2021, Distribution and origin of tectonic fractures in ultra-deep tight sandstone reservoirs: A case study of Keshen gas field, Kuqa foreland thrust belt, Tarim Basin [in Chinese with English abstract]: Oil and Gas Geology, v. 42, no. 2, p. 338–353.

Wang, X., J. Hou, S. Song, D. Wang, L. Gong, K. Ma, Y. Liu, Y. Li, and L. Yan, 2018, Combining pressure-controlled porosimetry and rate-controlled porosimetry to investigate the fractal characteristics of full-range pores in tight

oil reservoirs: Journal of Petroleum Science Engineering, v. 171, p. 353–361, doi:10.1016/j.petrol.2018.07.050.

Wang, X., Z. Jin, G. Chen, M. Peng, L. Huang, Z. Wang, L. Zeng, G. Lu, X. Du, and G. Liu, 2022, Multi-scale natural fracture prediction in continental shale oil reservoirs: A case study of the Fengcheng Formation in the Mahu Sag, Junggar Basin, China: Frontiers of Earth Science, v. 10, 929467, 15 p., doi:10.3389/feart.2022.929467.

Watkins, H., C. E. Bond, D. Healy, and R. W. H. Butler, 2015, Appraisal of fracture sampling methods and a new workflow to characterize heterogeneous fracture networks at outcrop: Journal of Structural Geology, v. 72, p. 67–82, doi:10.1016/j.jsg.2015.02.001.

Wu, H., and D. D. Pollard, 1995, An experimental study of the relationship between joint spacing and layer thickness: Journal of Structural Geology, v. 17, no. 6, p. 887–905, doi:10.1016/0191-8141(94)00099-L.

Wu, S., Z. Yang, S. Pan, J. Cui, S. Lin, L. Su, H. Bale, Y. Hong, and W. Shi, 2020, Three-dimensional imaging of fracture propagation in tight sandstones of the Upper Triassic Chang 7 member, Ordos Basin, Northern China: Marine and Petroleum Geology, v. 120, 10450, 11 p., doi:10.1016/j.marpetgeo.2020.104501.

Zanella, A., P. R. Cobbold, G. Ruffet, and H. A. Leanza, 2015, Geological evidence for fluid overpressure, hydraulic fracturing and strong heating during maturation and migration of hydrocarbons in Mesozoic rocks of the northern Neuquén Basin, Mendoza Province, Argentina: Journal of South American Earth Sciences, v. 62, p. 229–242, doi:10.1016/j.jsames.2015.06.006.

Zeng, L., 2010, Microfracturing in the Upper Triassic Sichuan Basin tight-gas sandstones: Tectonic, overpressure, and diagenetic origins: AAPG Bulletin, v. 94, no. 12, p. 1811–1825, doi:10.1306/06301009191.

Zeng, L., L. Gong, C. Guan, B. Zhang, Q. Wang, Q. Zeng, and W. Lyu, 2022, Natural fractures and their contribution to tight gas conglomerate reservoirs: A case study in the northwestern Sichuan Basin, China: Journal of Petroleum Science Engineering, v. 210, 110028, 10 p., doi:10.1016/j.petrol.2021.110028.

Zeng, L., and X. Li, 2009, Fractures in sandstone reservoirs with ultra-low permeability: A case study of the Upper Triassic Yanchang Formation in the Ordos Basin, China: AAPG Bulletin, v. 93, no. 4, p. 461–477, doi:10.1306/09240808047.

Zeng, L., and H. Liu, 2010, Influence of fractures on the development of low-permeability sandstone reservoirs: A case study from the Taizhao district, Daqing Oilfield, China: Journal of Petroleum Science Engineering, v. 72, no. 1–2, p. 120–127, doi:10.1016/j.petrol.2010.03.009.

Zeng, L., P. Lyu, X. Qu, and J. Fan, 2020, Multi-scale fractures in tight sandstone reservoirs with low permeability and geological conditions of their development [in Chinese with English abstract]: Oil & Gas Geology, v. 41, no. 3, p. 449–454, doi:10.11743/ogg20200301.

Zeng, L., W. Lyu, Y. Zhang, G. Liu, and S. Dong, 2021, The effect of multi-scale faults and fractures on oil enrichment and production in tight sandstone reservoirs: A case study in the Southwestern Ordos Basin, China: Frontiers of Earth Science, v. 9, 664629, 12 p., doi:10.3389/feart.2021.664629.

Zeng, L., H. Su, X. Tang, Y. Peng, and L. Gong, 2013, Fractured tight sandstone oil and gas reservoirs: A new play type in the Dongpu depression, Bohai Bay Basin, China: AAPG Bulletin, v. 97, no. 3, p. 363–377, doi:10.1306/09121212057.

Zeng, L., X. Tang, J. Qi, L. Gong, F. Yu, and T. Wang, 2012a, Insight into the Cenozoic tectonic evolution of the Qaidam Basin, northwest China from fracture information: International Journal of Earth Sciences, v. 101, no. 8, p. 2183–2191, doi:10.1007/s00531-012-0779-y.

Zeng, L., X. Tang, T. Wang, and L. Gong, 2012b, The influence of fracture cements in tight Paleogene saline lacustrine carbonate reservoirs, western Qaidam Basin, northwest China: AAPG Bulletin, v. 96, no. 11, p. 2003–2017, doi:10.1306/04181211090.

Zeng, L., J. Zhao, S. Zhu, W. Xiong, Y. He, and J. Chen, 2008, Impact of rock anisotropy on fracture development: Progress in Natural Science, v. 18, no. 11, p. 1403–1408, doi:10.1016/j.pnsc.2008.05.016.

Zhang, Y., L. Zeng, Q. Luo, R. Zhu, W. Lyu, D. Liu, Q. Dai, and S. Pan, 2021, Influence of natural fractures on tight oil migration and production: A case study of Permian Lucaogou Formation in Jimsar Sag, Junggar Basin, NW China: Journal of Earth Science, v. 32, no. 4, p. 927–945, doi:10.1007/s12583-021-1442-y.

Zhang, Y., L. Zeng, Q. Luo, R. Zhu, S. Pan, Q. Dai, J. Shi, J. Qin, and X. Xu, 2020, Effects of diagenesis on natural fractures in tight oil reservoirs: A case study of the Permian Lucaogou Formation in Jimusar Sag, Junggar Basin, NW China: Geological Journal, v. 55, no. 9, p. 6562–6579, doi:10.1002/gj.3822.

Zou, C., S. Tao, H. Zhou, X. Zhang, D. He, C. Zhou, L. Wang, et al., 2008, Genesis, classification, and evaluation method of diagenetic facies: Petroleum Exploration and Development, v. 35, no. 5, p. 526–540, doi:https://doi.org/10.1016/S1876-3804(09)60086-0.

Zucchi, M., A. Brogi, D. Liotta, A. Caggianelli, and A. Dini, G. Ventruti, G. Ruggieri, and P. F. Matera, 2022, Fractures, fluid flow and inherited structures in geothermal systems: Inputs from the Fe-ore deposits of eastern Elba Island (northern Apennines, Italy): Geological Magazine, v. 159, no. 11–12, p. 2238–2261, doi:10.1017/S0016756822000310.

Zucchi, M., A. Brogi, D. Liotta, V. Rimondi, G. Ruggieri, G. Montegrossi, A. Caggianelli, and A. Dini, 2017, Permeability and hydraulic conductivity of faulted micaschist in the eastern Elba Island exhumed geothermal system (Tyrrhenian Sea, Italy): Insights from Cala Stagnone: Geothermics, v. 70, no. 1, p. 125–145, doi:10.1016/j.geothermics.2017.05.007.